USING FEATURE EXTRACTION TO PERFORM EQUIPMENT HEALTH MONITORING ON SHIP-RADIATED NOISE

EXTRACTION DES CHARACTÉRISTIQUES DE NAVIRES PAR ANALYSE DES BRUITS RAYONNÉS À DES FINS D'ANALYSE DE L'ÉTAT DE L'ÉQUIPEMENT

A Thesis Submitted to the Division of Graduate Studies
of the Royal Military College of Canada
by

Nicholas Tomas Marasco, BEng, rmc
Lieutenant Commander

In Partial Fulfillment of the Requirements for the Degree of
Master of Applied Science in Electrical Engineering

March, 2023

To my wife Stacey, whose unfailing support during the past two years may be impossible to ever fully repay.

Acknowledgements

I would like to thank my supervisors, Dr. Elghamrawy and Dr. McGaughey for their expertise and encouragement, both of which proved instrumental in completing this project. I would also like to thank the sta at DRDC Atlantic, especially Jasper Dupuis, Layton Gilroy and Sean Pecknold for providing me the experimental data used to conduct this research and for making themselves routinely available to answer my questions.

Abstract

Ship radiated noise (SRN) has been an area of research for ship detection and classification for a number of years. A large number of feature extraction techniques have been developed and used in ship radiated noise analysis and have been shown to be highly effective at classifying vessels. There remains, however, limited research in the use of ship radiated noise as a medium for equipment health monitoring (EHM). If feature extraction techniques can be applied to a known vessel and shipboard equipment can be identified and tracked over time for evidence of defects, significant labour savings could be achieved by replacing the need for manually monitoring each system onboard.

In this thesis, the Fast Orthogonal Search (FOS) algorithm was selected and used as a high-resolution frequency analysis tool. It was used to extract features from examples of ship radiated noise from Patrol Craft, Training (PCT) Moose. The data was collected by the Defence Research and Development Centre (DRDC) and the Royal Canadian Navy's (RCN) Patricia Bay Hydroacoustic Range. Twenty-one individual systems were recorded and the aim of this thesis was to develop a method to identify and track each of them. Ultimately, 14 unique features were found, allowing 9 systems to be successfully classified, and one system was successfully tracked using the noise from a second acoustic recording that occurred six months after the initial training data was recorded. The results demonstrate that EHM using feature extraction techniques has excellent potential to identify and track discrete components of a ship using SRN and strongly support further research using more sophisticated feature extraction and classification techniques.

Résumé

Depuis de nombreuses années, le bruit rayonné par les navires fait l'objet de recherches dans le domaine de la détection et de la classification. Un grand nombre de techniques d'extraction des caractéristiques du spectre sonore ont été développées et utilisées dans l'analyse du bruit rayonné. Elles se sont avérées très e□caces pour la classification des navires. Il reste, cependant peu de recherches sur l'utilisation du bruit rayonné comme moyen de surveillance de l'état des équipements. Si des techniques d'extraction de caractéristiques peuvent être appliquées à un navire connu et que l'équipement de bord peut être identifié et suivi régulièrement pour la détection de signes de défauts, d'importantes économies de main-d'œuvre pourraient être réalisées en remplaçant la nécessité de surveiller manuellement chaque système à bord.

Pour la présente thèse, l'algorithme de recherche orthogonale rapide a été sélectionné et utilisé comme outil à haute précision d'analyse des fréquences sonores. Des caractéristiques sonores ont été extraites à partir de données collectées sur le patrouilleur d'instruction Moose (PCT 62) par Recherche et développement de la défense Canada (RDDC) et par le champ d'essai hydroacoustique de la baie Patricia de la Marine royale canadienne (MRC). En tout, 21 systèmes individuels ont été répertoriés. L'objectif de la présente thèse était de développer une méthode pour identifier et suivre l'évolution de chacun d'entre eux. Finalement, 14 caractéristiques uniques ont été trouvées, 9 systèmes ont été entièrement classifiées, et un système a été suivi avec succès en utilisant le bruit d'un deuxième enregistrement acoustique qui a eu lieu six mois plus tard après la collecte des données initiales. Les résultats démontrent que la surveillance de l'état des équipements par l'utilisation des techniques d'extraction de caractéristiques sonores sur le bruit rayonné par les navires à un excellent potentiel pour identifier et suivre l'évolution des composantes discrètes d'un navire. Ils justifient la poursuite des recherches utilisant des techniques d'extraction et de sélection de caractéristiques plus sophistiquées.

Contents

List of Tables

List of Figures

List of Acronyms

AM-FM	amplitude-modulated-frequency-modulated
BURNSi	Benchmark Underwater Radiated Noise Simulation
CEEMD	complementary ensemble empirical mode decomposition
CEEMDAN	complete ensemble empirical mode decomposition with adaptive noise
CEEMDASN	complete ensemble empirical mode decomposition with adaptive selective noise
CPA	closest point of approach
DAQ	data acquisition system
DG	diesel generator
DE	dispersion entropy
DFT	discrete Fourier transform
DRDC	Defence Research and Development Canada
DWT	discrete wavelet transform
EEMD	ensemble empirical mode decomposition
EHM	equipment health monitoring
EMD	empirical mode decomposition
FFT	fast Fourier transform
FOS	fast orthogonal search
FOS-FTR	fast orthogonal search with first term re-selection
FT	Fourier Transform
GPS	Global Positioning System
GS	Gram-Schmidt
IFOS	iterative fast orthogonal search
IMF	intrinsic mode function
MSE	mean square error
PCA	principle component analysis
PCT	patrol craft, training
PE	permutation entropy
RCN	Royal Canadian Navy

RDE	reverse dispersion entropy
RMS	root mean square
RPE	reverse permutation entropy
SRN	ship radiated noise
UWN	Underwater Noise
VA	vibration analysis
VMD	variational mode decomposition
WGN	white gaussian noise
WPE	weighted permutation entropy
WPD	wavelet packet decomposition
WT	wavelet transform

1 Introduction

The ability of sound to propagate in water has been known for centuries. Leonardo da Vinci commented in his notebooks that it is possible to hear distant ships by listening to the open end of a tube whose other end was placed in the water [1]. The technology would remain limited to rudimentary listening tubes until the nineteenth century, when the discovery of piezoelectricity [1] and the invention of the carbon button microphone made it possible to create the electronic hydrophone [2]. By the beginning of the twentieth century, systems utilizing passive listening and systems that used active sound transmission were being invented. These systems included a system for range estimation by comparing the difference in time of reception of in-water and out-of-water sound from a single known source, and an early use of echolocation for the detection of icebergs [2]. The outset of World War 1, however, spurred heavy research into hydro-acoustics, that progressed through the inter-war period and saw significant numbers of warships equipped for underwater detection and echolocation by the outset of World War 2 [2].

Research and improvements in the exploitation of underwater sound have continued since the end of World War 2. Military sonar systems have become more powerful and sensitive, allowing detection and ranging of quieter and more distant targets and acoustic technology has become widespread in non-military applications such as depth sounding, fish finding, side-scan sonar for ocean bottom mapping, communication and navigation [2].

In recent years, research interest has begun to look beyond simple detection into classification. The proliferation of data processing techniques has allowed deeper analysis of received acoustic signals. The question of whether ships can reliably be identified by class or specific vessel based solely on their acoustic noise has been probed by several researchers [3] [4] [5]. Using a variety of processing algorithms and machine learning techniques classification algorithms have been able to identify ships from a small set of candidates based only on their radiated noise with greater than 95% accuracy [3].

Naval warships, as with commercial ships, are seeing an increasing trend

toward integration of systems and the automation of monitoring and control, enabling a ship to operate with a much smaller crew. This leaves the remaining tasks that cannot be automated to be completed by a decreasing number of personnel. Simultaneously, the increased complexity of modern ship systems has led to increased maintenance requirements and difficulty in accurately diagnosing issues before equipment failure. Techniques such as oil particulate monitoring or the manual capture of vibration data are labour intensive, and it may not be possible to conduct them at the frequency required to predict equipment failure reliably. An innovative approach to equipment health monitoring (EHM) is required that reduces the labour cost for ship operators and maintainers and, if possible, improves the ability to forecast equipment failure.

The increased interest in the analysis of ship radiated acoustic signals has focused on a variety of techniques for performing feature extraction with the aim of conducting ship classification. It may therefore be possible to use feature extraction techniques to identify specific components of a known ship, allowing these components to be monitored over time for signs of degradation. This would enable EHM to be conducted holistically for the ship, rather than individually for each component. Further, as this data is collected in the radiated acoustic noise, it could be captured by personnel not actively operating the ship (i.e., by a repair and maintenance facility as a ship enters or leaves harbour) allowing the redistribution of maintenance tasks.

1.1 Problem Statement

The relationship between the noise and vibration generated by machinery and its mechanical health are well known and commonly exploited phenomenon. The Royal Canadian Navy (RCN) has policies in place that highlight the relationship between equipment health and generated acoustic noise and has directed routine EHM activities to exploit this relationship in the early detection of defects [6]. One such EHM activity specifically analyzes the vibration generated by rotating or reciprocating equipment in order to detect unusual vibrations and signal potential mechanical defects [7]. This maintenance is time consuming and requires sensitive, specialized vibration monitors. With the trend in ships towards more complex integrated systems and smaller crews, keeping up with EHM activities is becoming more challenging. If an approach can be found to identify defects in equipment in a more holistic, less time intensive manor, it could ease the maintenance burden on maintenance departments.

Given the accuracy of recently developed classification algorithms, it seems

reasonable to conclude that ship radiated noise (SRN) contains features that are stable in time, and are able to be detected reliably. The nature of SRN is well known and in particular it is known that ship machinery generates noise in the line component spectrum [2], in which specific frequencies are readily apparent. Many of these line component frequencies, especially those emanating from machinery not related to propulsion are generally stable in time. It is reasonable to assume that ship machinery noise, therefore, contributes to the features that current algorithms are detecting for ship classification.

If machinery noise forms part of the features being extracted for ship identification, a question arises whether these features can be identified and, if the ship is a known entity, they can be monitored for changes. The fast orthogonal search (FOS) algorithm is a signal estimation algorithm that can be used for spectral analysis, and has been experimentally shown to have much higher frequency resolution and be more effective at identifying line component spectra than the FFT[8]. As a result, it may be an ideal tool for feature extraction from SRN when the goal is the identification of ship's equipment.

Current EHM and vibration analysis (VA) techniques within the RCN focus on measurement and analysis of individual pieces of equipment. Feature extraction techniques present an opportunity to identify and track all mechanical equipment on a ship simultaneously, identifying defects on any piece of equipment as a deviation from the normal acoustic signature of the ship. The potential reduction in labour by monitoring all equipment simultaneously could significantly reduce the workload of maintenance departments. This conserved effort could be redirected to other tasks, improving the overall maintenance state of the ship. Additionally, since the data could be collected external to the ship, a repair facility such as the RCN's Fleet Maintenance Facilities could collect and analyze the data on the ships behalf, further reducing the maintenance strain on ship's crews

1.2 Research Objectives and Scope

The goal of this thesis is to use feature extraction techniques to identify discrete pieces of equipment from samples of the ships radiated noise and track them over time to conduct equipment health monitoring. The ability to reliably detect equipment, track that equipment over time, and determine if changes to that equipment are apparent from the ships noise will result in a tool for monitoring a ship's equipment health.

After a review of the relevant literature and a comparison of the relative strengths and weaknesses of common feature extraction techniques, the FOS

algorithm was chosen for feature extraction due to its excellence in identifying line spectrum tones and its high frequency resolution with short data samples [8].

1.3 Organization

This thesis is organized into six further chapters. Chapter 2 contains a discussion on the foundational topics on which this thesis is built. It contains a discussion on the nature of ship radiated noise and it's components, as well as examinations the properties of sound propagation in water. Chapter 3 contains a literature review that examines recent scholarly work in the area of feature extraction, examining the methods, advantages and weaknesses of recent feature extraction techniques as they relate to ship radiated noise. Specific attention is paid to the applicability of each technique for identifying specific equipment via SRN. Chapter 4 contains a detailed explanation of the FOS algorithm and its applications for signal estimation and spectral analysis. Chapter 5 details the experimental data that was collected from the Underwater Noise (UWN) and Benchmark Underwater Radiated Noise Simulation (BURNSi) trials. It described the experimental conditions, the methodology used during the trial, and the method of encoding and saving the data. Chapter 6 is a detailed explanation of the methodology used in this thesis to accomplish the stated goals, as well as an analysis of the results of the data processing and analysis. Finally, Chapter 7 contains a summary of the overall thesis and a conclusion on the results achieved and Chapter 8 contains potential future avenues to continue working on the use of FOS for EHM.

2 Background

2.1 Ship Radiated Noise

A ship is not a single source of noise, but rather a complex system of individual noise sources, comprising mechanical sources such as rotating machinery, noises from the propeller such as cavitation and propeller wash, and the hydrodynamic noise of the hull passing through the water [4] [9] [10]. Of these three noise sources, the mechanical and propeller noises, transmitted through the ship's hull and radiated into the water, comprise most of the detectable SRN [9] [10].

An example of the spectrum of SRN is provided at Figure 2.1. This example was drawn from the acoustic data collected by DRDC and provided for use in this thesis, and spectrally analysed using the FFT, with a sample time of 1s. Ship noise comprises line spectrum and continuous spectrum components. Line spectrum components, which contain energy concentrated in a narrow frequency, can be seen as the narrow peaks (e.g. at 70Hz) in the figure. Continuous, or broad, spectrum noise has energy spread across several frequencies and can be seen in the figure as sections of generally increased energy. The frequency range between 250Hz and 350Hz shows an example of continuous spectrum noise with occasional line spectrum components standing out from it.

2.1.1 Mechanical Noise

Mechanical noise is created by the various moving and rotating pieces of machinery within the ship. It is transmitted to the water via the ships structural components and radiates from the hull. Discontinuous or unbalanced rotating components, reciprocating components, cavitation, and friction between components all contribute to this noise [9]. This noise can be characterized by strong line spectra and weak continuous spectrum, where the frequency and amplitude of the spectra for main propulsion machinery will vary with

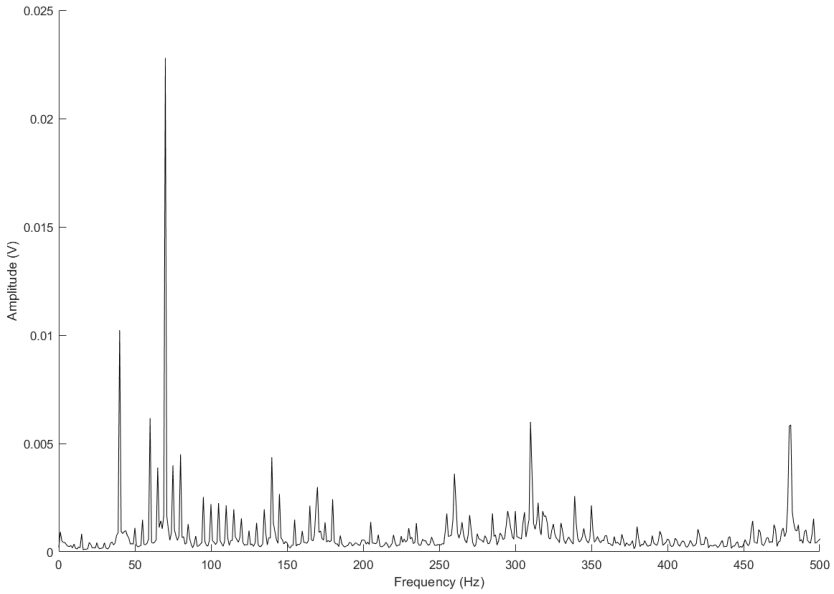

Figure 2.1: Example of the Ship Radiated Noise Spectrum

ship's speed and the line spectra for auxiliary machinery are more stable and independent of ship's speed [9].

2.1.2 Propeller Noise

While the propeller is a component of the main propulsion equipment chain, the noise generated by the propeller originates within the water as opposed to within the ships hull. Propeller noise also has unique characteristics, and it is therefore treated as an independent noise source. A propeller generates three distinct types of noise: cavitation sounds, rotation sounds, and resonance, or 'singing'. Cavitation is the production and subsequent bursting of bubbles as the propeller blades pass through the water. Because the creation and bursting of the bubbles is essentially random, the noise generated is continuous spectrum and spans a broad frequency range [9]. This noise will have a peak somewhere in the 100-1000Hz range, which will increase in both frequency and amplitude with the ship's speed [9]. However, below certain rotation speeds (which vary based on the propeller characteristics) cavitation does not occur and this noise is not present. In contrast, at high speeds, cavitation noise is

strong enough that the continuous spectrum noise it generates can overpower other noise sources.

Resonance, or singing is a resonant noise generated by the propeller blades slapping and cutting through the water. This noise is low frequency in nature and appears as a line spectrum in the frequency domain [9].

2.1.3 The Ship Radiated Noise Model

Both the mechanical and propeller noise generated by a ship are continuous spectra in the frequency domain with superimposed line spectra. As a result, a simple model of SRN can be a summation of the continuous spectrum noise and the line spectra noise and can be represented by the formula [10]:

$$S(t) = S_x(t) + S_l(t) \tag{2.1}$$

where $S_x(t)$ represents the continuous spectrum noise and $S_l(t)$ represents the line spectrum noise.

2.2 Sound Transmission in Water

There are several factors that a□ect the propagation of sound in water. The speed of sound in any fluid is generally described as [1]:

$$c = \sqrt{\frac{K}{p_0}} \tag{2.2}$$

where K is the bulk modulus, and p_0 is the equilibrium density for that fluid. There are several other factors that a□ect the speed of sound in seawater, however, varying with the following relationships[2][1]:

1. in the temperature ranges found in the ocean, the speed of sound increases with increasing temperature by approximately $5\frac{m}{s}/^{\circ}C$;
2. the speed of sound increases by approximately $1\frac{m}{s}$ for every part per thousand increase in salinity; and
3. the speed of sound in water increases with hydrostatic pressure by approximately $1.6 \quad 10^{\ 6}\frac{m}{s}/Pa$

Variations in the speed of sound in water can drive phenomenon such as ray bending, where the direction of travel of the sound tends to bend toward areas of localized minimum speed of sound. In extremes, this can cause sound to fail to penetrate out of specific depth regions. Due to the confined nature of the Patricia Bay Range, where the data was collected, and the short travel distance

of the sound being studied from the source to the hydrophones, it is expected that variations in the speed of sound during this trial will be extremely small and will therefore have a negligible result on the collection and processing of the data.

2.2.1 Losses

The intensity of sound, L_p is measured in dB and can be calculated by the formula [1]

$$L_p = 20 \log_{10} \frac{p_{rms}}{p_{ref}} \tag{2.3}$$

where p_{rms} is the root mean square (RMS) pressure of the wave and p_{ref} is a reference pressure. For water, the standard p_{ref} is $1\mu Pa$. Factors that lead to sound intensity losses include dispersion, and absorption. Dispersion is caused by a wavefront expanding in all directions and the energy in that wave is spread out spherically. This results in a relative loss of sound intensity that is proportional to the square of the distance that the wave has travelled. These losses can be calculates by the formula[1]:

$$I(r) = \frac{W}{4\pi r^2} \tag{2.4}$$

where $I(r)$ is the sound intensity at a given distance, r, and W is the initial power of the sound.

Absorption occurs when some of the energy in the wave is absorbed by the water and converted to heat. This e□ect is also proportional to the distance the wave has travelled.

The static range trials that were used for much of this thesis were conducted with PCT Moose at a static distance of 100m from the hydrophones. While the DRDC reports explain that the ship was anchored in place, rather than the more fixed four-point mooring normally used, the variations in distance caused by this were not measured, nor was the sound level at 1m from the ship, which would normally be used as a baseline for calculating sound intensity losses. As with the previous section, given the small size of the acoustic range and reasonably static conditions of the trials, it is not expected that any losses negatively impacted the collection or processing of the data.

2.2.2 Wave Distortion

As previously stated, the speed of sound in water increases with pressure. This causes an e□ect where sound waves do not travel at uniform speeds. Due

to this effect, the pressure peaks of a sound wave will travel slightly faster than its troughs [1]. Over enough time, the peaks will begin to encroach on the troughs and distort the original sinusoid, creating a discontinuity between the half-cycles of the sound wave and generating a shock wave. If this wave continues, the advance of the pressure peaks begins to dissipate the shock wave. The shock wave has effectively converted some of the energy of the original sinusoid to a higher frequency, which attenuates more quickly than the lower frequency energy and the travelling wave eventually decays to a lower amplitude sinusoid [1]. This cycle then repeats as the wave travels further.

The effect of this phenomenon on spectral analysis is that, as the wave discontinuity grows, several harmonics of the original pure sinusoid develop. As the shock wave develops, wide band noise begins to develop around the wave frequency. Both the noise and the harmonics dissipate as the wave continues to travel and reverts back to a lower amplitude sinusoid at the original frequency [1].

While this effect will not have time to develop significantly on the noise radiated form PCT Moose, the same cannot be said of the background noise. Background noise comprises numerous individual noise sources at various distances to the Patricia Bay Range, and as a result it can be assumed that it will contain tones, harmonics and broadband noise and that these effects will vary in terms of both frequency and magnitude over time. Chapter 6 contains detailed discussion on how the FOS algorithm was used to manage the effects of this noise.

2.3 The Fourier Transform and Spectrograms

The Fourier Transform (FT) is used in this thesis as a tool to verify the results of research activities that employ spectral analysis and as a means to easily generate frequency domain data. It is a well known technique for translating time series data into the frequency domain, the formula for which is given by[11]:

$$X(f) = \mathcal{F}\{x(t)\} = \int_{-\infty}^{\infty} x(t) e^{-2\pi f t} dt \tag{2.5}$$

where $X(f)$ is the frequency series or spectrum of a time series signal, $\mathcal{F}$ represents the FT, and $x(t)$ is the time series. The result of this calculation is complex and is usually separated into a magnitude and a phase spectrum [11]. The FT is a continuous transform and must be discretized for use with digitally

sampled systems. This is known as the discrete Fourier transform (DFT) and is calculated using the formula [11]:

$$X_s(k) = \sum_{n=0}^{N\ 1} x_s(n) e^{\ j2\pi kn/N} \tag{2.6}$$

where n represents the samples, and k represents the digital frequency. MATLAB contains a fast Fourier transform (FFT) function, which is an optimized algorithm for calculating the DFT. The results are mathematically identical to the DFT [11].

A spectrogram is a graphical representation of frequency domain data as it varies in time. This is normally presented as a three-axis plot with the axes representing time, frequency and magnitude. One method of producing a spectrogram is to perform a series of FT on successive segments of a time series. Arranging the results of each FT along a time axis produces a spectrogram. The spectrogram can be arranged strictly consecutively, or segments can be processed by averaging or overlapping for each time row. Figure 5.2 contains an example of a spectrogram used in this thesis, where frequencies are plotted on the x-axis, time is plotted on the y-axis and magnitude is represented as a colour scale for varying intensities in order to plot the information in 2 dimensions.

2.4 Confusion Matrices

The results of classifier testing will be presented within this thesis in a table called a confusion matrix. A classifier maps tested samples into classes. In the case of a binary classifier, as will be used in these research activities where the possible classes are simply a positive or negative estimation, there are four possible outcomes. These four results correspond with the combinations of the two possible estimated classes, and the two true classes[12]. For clarity, estimated classes will be referred to as 'positive' and 'negative' while true classes will be referred to as 'yes' and 'no'. Table 2.1 demonstrates an example confusion matrix with a count of each of the four possible outcomes displayed in one cell of the table. The sum of all 'yes' (Y) and 'no' (N) classes, denoted here as M, is displayed in a separate cell for quick reference.

From a confusion matrix, the performance of the classifier can be determined using the following relationships[12]:

a) The false positive rate is the ratio of false positive results to the total number of 'no' samples;

Table 2.1: Example Confusion Matrix

		Estimated Class	
	Total Samples Y+N = M	Positive	Negative
True Class	Yes	True Positive	False Negative
	No	False Positive	True Negative

b) The false negative rate is the ratio of false negative results to the total number of 'yes' samples; and
c) The total probability of error is given by the formula:

$$Pe = P(y)P(Ejy) + P(n)P(Ejn) \tag{2.7}$$

3 Literature Survey

3.1 Feature Extraction Techniques

In recent years a wealth of proposed techniques have arisen to address the challenge of feature extraction from SRN. While the individual techniques are numerous, they generally follow three main approaches [5]. The first approach is to analyze the noise directly in the time or frequency domain and attempt to build a representative signal for the SRN [5][13]. The second approach is to decompose the SRN into intrinsic mode functions (IMFs). Comparisons between the IMFs such as energy difference between the frequencies or changes in energy between the IMFs can be used as characteristic parameters for the SRN [5]. Finally, the signal can be decomposed into IMFs as in the previous method, however this time a single IMF can be selected as representative of the SRN and it can be analyzed for characteristic parameters, such as center frequency or energy entropy [14] [15]. While a full review of each novel technique would be impossible, the following is a short review of some of the techniques being utilized as a representative sample.

3.1.1 Wavelet Packet Decomposition

The wavelet transform (WT) is a time frequency signal analysis technique that uses a series of scaled versions of a base, or mother wavelet, which are translated in time to transform an input signal. The formula for this transformation is given by [16]:

$$CWT(a,\tau) = 1/\sqrt{a} \int_{1}^{1} S(t)\psi\left(\frac{t-\tau}{a}\right) dt \tag{3.1}$$

where S is the input signal, t denotes the time in seconds,ψ is the wavelet function, a is the wavelet scaling factor and, τ is translation of the wavelet. Performing this transformation results in the cross-correlation of the wavelet

as a function of both the translation of the wavelet (and therefore the time) and the scaling of the wavelet (which inversely correspond to frequencies).

Calculating a continuous function such as this is costly in terms of processing power and produces far more data than can quickly be processed. As a result, this process can be discretized, by limiting τ and a to discrete terms. The Discrete discrete wavelet transform (DWT) then becomes:

$$DWT(a,b) = \frac{1}{b} \sum_{m=0}^{p} S(t_m)\psi\left(\frac{t_m - a}{b}\right) dt \tag{3.2}$$

where a and b now represent the discrete τ and a respectively [16]. Functionally, this decomposition can then be conducted by passing the signal through a high and low pass filter to obtain coefficients for the wavelet (for time details) and for the scaling factor. Repeating this process on the output of the low pass filter produces a series of data bands that can then be analyzed for identifying features of SRN, such as the relative energy between bands. This has been shown to be reasonably effective in conducting SRN based ship recognition [5].

Newer techniques have been developed that expand on the WT and improve its effectiveness at ship recognition. One such technique is to perform wavelet packet decomposition (WPD). Where wavelet decomposition normally focuses on only the low pass filtering, identifying the underlying shape of the signal and filtering out high frequency information as noise, WPD performs wavelet filtering in both high and low pass stages [3]. This results in each stage of decomposition generating two bands from the previous stage. Figure 3.1 shows a graphical representation of the WPD algorithm using 3 layers of decomposition where $\mu(x)$ represents the time domain signal. The wavelet coefficients for each level of decomposition (n) and frequency band (k) are then represented as $\mu_{n,k}$, and h and g represent the low and high pass filters that generate the decompositions. $\mu_{0,0}$ therefore represents the wavelet function and $\mu_{0,1}$ the scaling function. Each band represents a time domain signal at a unique frequency range. The previous frequency band in the decomposition can be reconstituted by adding the two resulting bands together, and the original time series can be similarly reconstituted by summation of all decomposition bands at any layer.

After using this more detailed decomposition a variety of feature extraction methods can be applied, such as energy entropy (i.e., the variation in energy within the various bands), center frequency, and permutation entropy [3]. Coupled with energy entropy for feature extraction, the WPD technique has been shown to be up to 98% effective at classifying SRN [3]. A more

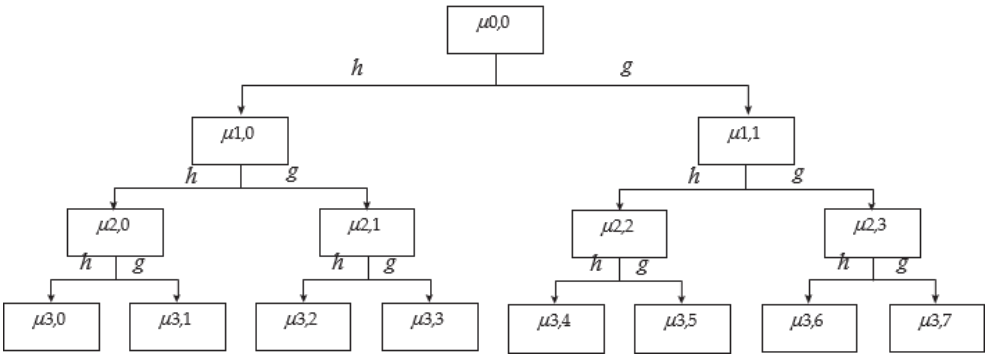

Figure 3.1: Three Layer Wavelet Packet Decomposition [3]

detailed analysis of entropy techniques for feature extraction can be found in Subsection 3.1.5.

3.1.2 Emprical Mode Decomposition

Empirical mode decomposition (EMD) is a technique for generating IMFs from a sample signal first proposed by Huang et al [17]. These IMFs are based on the concept of a signal's modes, which are here treated as a signal with the same number of zero crossings as it has maxima and minima (or a difference of at most one extreme or zero crossing) [17]. These IMFs are generated through a multi-step process, known as sifting:

a) The input signal is analyzed and all local maxima and minima (i.e. all peaks and troughs) are identified;
b) Upper and Lower envelopes are generated for the maxima and minima using spline interpolation;
c) The mean of the upper and lower envelope is calculated;
d) The envelope mean is subtracted from the signal to produce a residual signal;
e) The residual signal is compared against the pre-established requirements to determine if it is a valid IMF;
f) If the residual is not a valid IMF, the sifting process is repeated, using the residual as the signal, until the resulting residual is a valid IMF; and
g) Once a valid IMF is gained, it is subtracted from the original signal to produce a new, modified signal.

Repeating this process on the modified signal several times results in a series of IMFs of successively lower frequency information. The collection

of IMFs can be recombined with the remaining residual to reconstitute the original signal, proving that it is a complete decomposition technique, and no data is lost [17]. Following the EMD, the IMFs can then be analyzed for features. The application of the Hilbert Transform to the IMFs, for example, allows the instantaneous frequencies of each IMF to be computed [17].

While this technique has been widely used, it does su□er from a phenomenon known as mode mixing. Mode mixing occurs when a signal contains a mode which does not contain any clear local maxima or minima, and, as a result, its data is captured within another mode's IMF. Several techniques have been developed to expand on the EMD to produce improved decomposition results. These techniques include ensemble empirical mode decomposition (EEMD) [5], complementary ensemble empirical mode decomposition (CEEMD) [18], complete ensemble empirical mode decomposition with adaptive noise (CEEMDAN) [19][20], and complete ensemble empirical mode decomposition with adaptive selective noise (CEEMDASN) [5].

3.1.3 Variational Mode Decomposition

Variational mode decomposition (VMD) was first proposed by K. Dragomiretskiy and D. Zosso as an alternative to established decomposition methods [21]. The method was designed to fix a variety of shortfalls in other approaches, such as the lack of a strong mathematical theory in EMD, the bandwidth limitations of wavelet transforms, and the inability of many methods to properly manage noisy signals [21].

VMD redefines the IMF proposed in the EMD technique into a more mathematical function where an IMF is an amplitude-modulated-frequency-modulated (AM-FM) signal that can be written as:

$$u_k(t) = A_k(t)\cos\phi_k(t) \tag{3.3}$$

where $\phi_k(t)$ is the phase and is a non-decreasing function, $A_k(t)$ is the envelope and is non-negative, and the envelope and instantaneous frequency both vary significantly more slowly than the phase [21]. Requiring $\phi_k(t)$ to be non-decreasing allows $\phi_k^{0}(t)$, the instantaneous frequency to remain positive. Over carefully selected intervals, the modes can be considered to be pure harmonic signals, where $A_k(t)$ and $\phi_k^{0}(t)$ describe the mode's amplitude and instantaneous frequency, respectively [21]. Dragomiretskiy and Zosso detail the exact mathematics for the VMD process in [21], but the general process for VMD is as follows:

a) The input signal is decomposed into a series of bandwidth limited modes, whose bandwidth is estimated via Gauss Smooth Demodulation [21];
b) The mode is then frequency shifted to the current center frequency estimate, and a Wiener filter is applied about the current center frequency estimate [21]; and
c) A Lagrangian Multiplier is applied to the IMF to ensure that the IMFs maintain the ability to exactly reproduce the original signal [21].

Experimentally, VMD has repeatedly shown to be more effective than EMD in detection and separation of tones and with its ability to filter through noise [21] [22]. Some shortfalls of the VMD approach include the requirement to break down time varying signals into small, relatively non-varying segments, as the process is only able to adequately process stationary signals. VMD also requires the number of modes to be pre-defined, which has a limiting effect on the ability of this method to be used for unknown signals.

3.1.4 Complexity

The analysis of a signal's complexity is another heavily researched method for feature extraction with SRN. The basic premise is that any given ship will radiate a combination of periodic and random noise and the specific combination of these noises can be used to identify the ship [23]. One example of this technique is permutation entropy (PE).

The formula for nth order PE of a signal is given by

$$H(n) = \sum_{n} p(\pi) \log p(\pi) \tag{3.4}$$

where $H(n)$ represents a numerical value for PE. This value is between 0 and $\log n!$, where $H(n) = 0$ would represent a perfectly ordered signal (entropy is either continuously increasing or decreasing) and $H(n) = \log n!$ represents a signal with completely random entropy[23]. The symbol π represents the possible arrangements of the n samples in an n^{th} order PE. For example, in a 3^{rd} order PE, π can take one of eight permutations of the digits 0,1 and 2, to represent the relative entropies in the $n = 3$ samples being tested [23]. If the 3 samples are iteratively increasing in entropy, π would be (012) and if they were decreasing, it would be (210).

For a PE of order 2 the practical calculation would be conducted as follows:

a) The signal is broken into sample pairs and the pairs are compared and given $\pi = 01$ if the magnitude of the second sample is larger than the first, or $\pi = 10$ if it is smaller;

b) $p(01)$ and $p(10)$ then become the sum of sample sets that were given each π value divided by the total number of sample sets; and
c) PE for order 2 can then be calculated using equation Equation 3.4.

This process can be conducted for any order value, where increasing the order will increase the number of possible permutations and therefore the calculation time.

Initial research in PE showed that the calculations were extremely fast and this method was therefore a good technique for large data sets with little or no pre-processing [23].

Further improvements on PE have been developed since the introduction of the technique. Weighted permutation entropy (WPE) adds a weighting factor consideration on each sample to further differentiate the various permutations when conducting PE [24]. Dispersion entropy (DE) was then introduced which builds again on the PE technique by remapping sampled points using the normal cumulative distribution function before performing entropy calculations, which provides even more granularity in differentiating the signal [25]. Finally, reverse permutation entropy (RPE) was introduced which relies on the difference between the signal's permutations and white noise (i.e. noise where all permutations are equally likely) and reverse dispersion entropy (RDE) which combines the features of DE and RPE [26] [27].

3.1.5 Mixed Methods

As alluded to in Subsection 3.1.1, much current research in SRN and feature extraction has opted to combine various techniques to balance the relative strengths and weaknesses of each technique and to provide increased fidelity or granularity to the process. For example, combining WPD with PE allows PE to be performed on several frequency bands of a given SRN which allows greater differentiation, as two ships with similar overall PE may not share those characteristics over the same frequency ranges. The success rate of these combined techniques for classifying SRN is extremely high [3] [15].

3.1.6 Machine Learning

Machine learning algorithms use training data to allow a computer to build a model of the data being sampled. New data is then compared to the model and the resulting comparison is used as the basis for a classifier. The advantage of machine learning over other techniques is that machine learning algorithms are capable of processing vast quantities of data, producing models that would be difficult to create using conventional algorithms. Combining machine learning

with feature extraction techniques allows a high degree of complexity and accuracy to be achieved by classifiers. In fact, research that achieved 98% accuracy in ship classification did so by the combination of Energy Entropy for feature extraction with machine learning algorithms[3]. While the application of machine learning algorithms was not in the scope of this thesis, is is discussed in Chapter 8 that further research in the application of FOS based feature extraction techniques to SRN will require more sophisticated data processing, which can be provided by machine learning.

3.1.7 The Fast Orthogonal Search

FOS is a signal estimation algorithm that seeks to approximate an input signal using one or more pre-determined candidate functions. These candidate functions are fitted using a statistical correlation between the candidate function and the input signal.The candidate term that fits the most energy in the input signal is selected as the first fitted term in the estimation. Subsequent terms are added to the estimation in order to continue reducing the mean square error (MSE) between the estimation and the input signal until a preset threshold has been reached. This threshold can be the required amount of the original signal's energy that has been fitted, or a limit on the number of fitted candidate functions, or the algorithm can stop if it determines it is reducing the overall MSE by no more than if it were fitting white gaussian noise (WGN). A detailed explanation of FOS can be found in Chapter 4.

Spectral analysis via the FOS has been shown experimentally to have a frequency resolution up to 10 times that of the Fast Fourier Transform, making it extremely useful for very fine frequency analysis and signal reconstruction [8]. If spectral analysis is not necessary, the FOS remains a very flexible tool for signal estimation and reconstruction. In fact, spectral analysis is a special case use of the FOS algorithms original purpose, which is time series estimation. Since the goal is the estimation of the sample signal, the exact frequencies contained become of lesser importance and the candidate functions can be comprised of any arbitrary set of functions. These functions need not even be mathematically constructed; the FOS algorithm can be programmed to use sampled signals as the candidate functions. Section 3.3 will explain how the use of FOS can be applied to EHM.

3.2 Fault Detection

EHM and fault detection in machinery is a mature area of research, owing to the obvious economic advantages in being able to circumvent machinery

failure or maximize equipment reliability in an industrial setting. As a result, there are a variety of methods for monitoring rotating machinery for signs of impending failure. These include electromagnetic field monitoring, vibration analysis (VA), acoustic noise monitoring, motor current signature analysis, and a variety of other techniques [28]. All these techniques are best suited to monitoring di□erent aspects of equipment health.

A common use for VA is to monitor bearing health, as failing bearings will introduce unbalanced rotation and therefore vibrations in the machine. Since bearings are common to all rotating machinery, and nearly half of all motor failures are related to failed bearings [28] it can be concluded that VA is an important monitoring tool for any rotating machinery. This is further supported by the RCN adoption of VA for EHM for all rotating machinery that was previously discussed.

Additionally, due to VA being a relatively mature EHM technique, the e□ects of defects on bearings are well understood and the vibration resulting from a defect on a ball bearing can be calculated. For example, a ball bearing may experience defects on the races, the balls or the train. For each of these, the resulting vibration can be calculated as follows [28]:

$$f_{v(innerrace)} = \left(\frac{N}{2}\right) f_r[1 \quad \frac{d_b \cos(\beta)}{d_p}] \tag{3.5}$$

$$f_{v(outerrace)} = \left(\frac{N}{2}\right) f_r[1 + \frac{d_b \cos(\beta)}{d_p}] \tag{3.6}$$

$$f_{v(ball)} = \frac{d_p f_r}{2 d_b} \left(1 \quad [\frac{d_b \cos\beta}{d_p}]^2\right) \tag{3.7}$$

$$f_{v(train)} = \left(\frac{f_r}{2}\right) [1 \quad \frac{d_b \cos\beta}{d_p}] \tag{3.8}$$

where f_v is the vibration frequency, f_r is the rotational frequency of the machine, N is the number of balls in the bearing, d_b is the ball diameter, d_p is the pitch diameter and β is the contact angle between the balls and the races [28]. These frequencies can therefore be calculated for any ball bearings on the equipment being monitored and the presence of energy at those frequencies when conducting VA could be an indication a defect in the associated component.

3.3 Equipment Health Monitoring using Ship Radiated Noise

In order to determine the viability of the various SRN techniques for use in EHM, it is important to first generate a series of assumptions on how the EHM will be conducted:

a) EHM will be conducted on a known ship. That is, the data will be drawn in such a way as to positively identify the ship as the data is collected. A good example, and the assumption that will be used for this thesis, is that the acoustic signature of the ship will be recorded as the ship enters or leaves harbour;
b) The equipment on the ship will be known. That is, the characteristics of the bearings and or VA data conducted on the individual components can be accessed; and
c) Analysis techniques are not time constrained (i.e. EHM does not have to be conducted in real-time).

Radiated noise from a ship is composed of machinery noise, hydrodynamic noise and propeller noise. Hydrodynamic noise is a small component of the overall signal and is often masked by the other noise sources. It was also shown that the propeller noise varies in direct relation to the speed of the ship. Harbours in general, and certainly those operated by the RCN, are controlled areas where limits on wake are enforced, limiting ship speeds. This, coupled with the restricted navigation options a□orded by narrow harbour channels, allows an assumption that ships entering and leaving harbour will be moving slowly and are unlikely to rapidly accelerate or decelerate. As a result, it can be expected that the ship will be generating relatively little propeller noise and the ship's radiated noise will therefore compromise predominantly machinery noise

In Chapter 2, machinery noise was described as comprising of strong discrete frequencies and low-level continuous noise. Noise from propulsion machinery was said to vary with the ship's speed, while the remainder of the machinery was said to be unvarying in frequency and amplitude. Since the ship is assumed to be moving at a constant speed at the time of collection, it can be assumed that all collected noise will be non-varying in frequency and amplitude.

While at first this may seem to be an ideal scenario in terms of EHM, it presents several problems for the reviewed methods of feature extraction for SRN. Empirical mode decomposition and the various complexity techniques for feature extraction assume a time varying signal. That is, they expect the

line spectrum components to vary between successive samples. In fact, they rely on the variation of the signal over time to generate features. Since much of the research in SRN has been aimed at ship classification, the assumptions upon which the techniques were built are inherently different. EMD, and complexity analysis assume an unknown vessel operating dynamically and therefore will be producing much more propeller noise and varying machinery noise. While this is very effective for whole ship classification, it will not be effective at isolating single equipment sources.

VMD does assume a time-invariant signal and has been shown to deconstruct complex signals with better detection and separation of tones, and better noise filtering than EMD [21]. As a result, there is a possibility for further research into VMD for use in EHM for SRN, however there is an inherent bandwidth limitation on the deconstructed modes using VMD [21]. This may cause difficulty in analyzing harmonics created by unbalanced loads. As a result, further research using VMD was not be pursued.

The remaining techniques are those that analyze the time-frequency domain directly. In this thesis, the WT and its derivative techniques and the FOS was reviewed. The more advanced methods of WPD are normally coupled with other feature extraction techniques, but the WT on its own is a pure time-frequency analysis tool. As a result, it could be used in as a tool for EHM. Its drawbacks, however, are that significant processing is done to analyze the signal in both the time and frequency domains and it has been established that our signals are expected to be relatively stable in the time domain.

FOS is a computationally expensive analysis tool. The process of fitting the orthogonal functions is iterative and therefore time consuming. However, the extra calculations done by the algorithm provide significant advantages in terms of its ability to analyze a signal with significantly shorter sample times than with other techniques [29]. Thus, even a slowly varying SRN could be briefly sampled to produce an approximately time-invariant signal. Additionally, the FOS algorithm maintains superior frequency resolution to similar spectral analysis tools. Since the intent is to analyze SRN holistically, good frequency resolution will be essential. Many of the rotating machinery components onboard the ship will have similar rotational frequencies or be rotating at multiples of the same frequency. While it may be impossible to separate some machinery if they are rotating at the same frequency, FOS presents a good possibility of detecting minute frequency differences and therefore stands a good chance to separate equipment even at very close frequencies.

Lastly, since FOS algorithm is a signal estimation tool that can be used in a spectral analysis capacity, it can also bypass spectral analysis and directly

estimate a given signal with little or no modification to the underlying algorithm. Given the assumption that the individual components of the machinery noise are known, it can be assumed that they can be measured through VA or calculated using known properties of rotating machinery as shown with the vibrational frequencies of defects in ball bearings. These individual machinery components can then be used as the arbitrary functions for reconstruction of the SRN using FOS. The inability of FOS to fit an arbitrary function that was built using VA data could indicate that the equipment has a defect that has altered its vibration signature. In the case of arbitrary functions created using mathematical failure modeling, an indication of failure would be present if the FOS algorithm assigns significant weight to that function in the reconstruction. Finally, a trend over time of increasing or decreasing weight being given to an arbitrary function could also be used as an indication that equipment health is degrading.

Based on the flexibility of FOS in conducting spectral analysis or signal reconstruction, and the several possible means of detecting equipment defects in SRN, there is compelling reason to conduct further research.

4 Applying the Fast Orthogonal Search to Ship Radiated Noise

4.1 The Fast Orthogonal Search

The FOS algorithm is a technique for modelling a signal that estimates the functional expansion of a given signal based on a set of arbitrary candidate functions [30]. The formula for this expansion is given by [31]:

$$y(n) = \sum_{m=0}^{M} a_m p_m(n) + e(n) \tag{4.1}$$

where $y(n)$ is the input signal, a_m is the weight assigned to the arbitrary function $p_m(n)$ and $e(n)$ is a residual error.

4.1.1 Orthogonalization

The arbitrary functions are not orthogonal; therefore, the algorithm first fits a series of orthogonal functions according to the following formula [31]:

$$y(n) = \sum_{m=0}^{M} g_m w_m(n) + \varepsilon(n) \tag{4.2}$$

where $w_m(n)$ are the orthogonal functions, g_m are the orthogonal weights, and $\varepsilon(n)$ is the residual error. The orthogonal functions are derived from the arbitrary candidate functions via Gram-Schmidt (GS) orthogonalization [30]. The formula for this process is given by

$$w_m(n) = p_m(n) \quad \sum_{i=0}^{m\ \ 1} \alpha_{mi} w_i(n) \tag{4.3}$$

where α_{mi} are GS orthogonalization weights and the other variables are as in equations Equation 4.2 and Equation 4.3. The GS orthogonalization weight for any arbitrary function p_m and any orthogonal function w_r, denoted α_{mr} is calculated using the formula [31]:

$$\alpha_{mr} = \frac{\overline{p_m(n)w_r(n)}}{\overline{w_r^2(n)}} \tag{4.4}$$

Two processes, x(t) and y(t) are considered orthogonal if their summation over a specified interval is zero, meaning that there is no common energy between the functions. The process of GS orthogonalization ensures that the orthogonal functions have no common energy between them by removing the energy of all previous functions to each successive function as it is orthogonalized. Therefore, by converting the candidate functions to orthogonal functions, it is ensured that when a function is fit, it is fitting only the energy that is unique to that function and not fitting energy that has previously been fit.

4.1.2 Implicit Calculation

To speed up the FOS algorithm, the orthogonal functions can be implicitly calculated using the variable $D(m,r)$ which is defined as [31]:

$$D(m,r) = \overline{p_m(n)w_r(n)} \tag{4.5}$$

The correlation of $\overline{p_m(n)w_r(n)}$ does not need to be computed point-by-point. It can be calculated iteratively by modification of equation Equation 4.3 [31]:

$$\overline{p_m(n)w_r(n)} = \overline{p_m(n)p_r(n)} \quad \sum_{i=0}^{r\ 1} a_{ri}\overline{p_m(n)w_i(n)} \tag{4.6}$$

which can then be simplified to yield

$$D(m,r) = \overline{p_m(n)p_r(n)} \quad \sum_{i=0}^{r\ 1} a_{ri}D(r,i) \tag{4.7}$$

Similarly, $\overline{w_r^2(n)}$ can also be calculated iteratively using

$$\overline{w_r(n)w_r(n)} = \overline{p_m(n)p_r(n)} \quad \sum_{i=0}^{r\ 1} a_{ri}\overline{w_r(n)w_i(n)} \tag{4.8}$$

which can be simplified using the results from equation Equation 4.7 to show

$$D(r,r) = \overline{w_r^2(n)} \tag{4.9}$$

Finally, equations Equation 4.5 and Equation 4.9 can be substituted into equation Equation 4.4 to give an implicitly calculated a_{mr}

$$a_{mr} = \frac{\overline{p_m(n)w_r(n)}}{\overline{w_r^2(n)}} = \frac{D(m,r)}{D(r,r)} \tag{4.10}$$

When comparing the model to the original input of the signal, Equation 4.1 can be rearranged and modified to yield the expression for the MSE of the model [32]:

$$MSE = \overline{\left[y(n) \quad \sum_{m=0}^{M} a_m p_m(n)\right]^2} \tag{4.11}$$

This relationship remains true following GS othogonalization, and the MSE of the system can therefore also be expressed as [32]:

$$\begin{aligned} MSE &= \overline{\left[y(n) \quad \sum_{m=0}^{M} g_m w_m(n)\right]^2} \\ &= \overline{y^2(n)} \quad \sum_{m=0}^{M} g_m^2 \overline{w_m^2(n)} \end{aligned} \tag{4.12}$$

The orthogonal functions g_m values for each candidate function are selected to minimize the MSE, which can be achieved by rearrangement of Equation 4.12[31]:

$$g_m = \frac{\overline{y(n)w_m(n)}}{\overline{w_m^2(n)}} \tag{4.13}$$

Since $w_m(n)$ is created implicitly, is it necessary to perform a similar series of calculations to find g_m. This is done through the creation of $C(m)$, which is defined as [31]

$$C(m) = \overline{y(n)w_m(n)} \tag{4.14}$$

As was shown above $\overline{y(n)w_m(n)}$ can be calculated recursively

$$\overline{y(n)w_m(n)} = \overline{y(n)p_m(n)} \quad \sum_{r=0}^{m\ \ 1} a_{mr} \overline{y(n)w_r(n)} \tag{4.15}$$

which can be simplified to

$$C(m) = \overline{y(n)p_m(n)} \quad \sum_{i=0}^{m \quad 1} a_{mi}C(i) \tag{4.16}$$

With $C(m)$ calculated, it can be substituted into equation Equation 4.13 to yield a calculation of g_m that uses the implicit calculations.

$$g_m = \frac{C(m)}{D(m,m)} \tag{4.17}$$

4.1.3 D(m,m) Threshold

Equation 4.7 shows that $D(m,r)$ is derived iteratively as the correlation of the current and previous candidate functions, combined with the sum of the products of all previous α_{ri} and $D(r,i)$ terms. Further, α_{mr} is implicitly calculated as the division of $D(m,r)$ and $D(r,r)$.

An issue can arise in situations where candidate functions are very closely correlated, as in the case when using FOS for spectral analysis, where the candidate functions have small frequency di□erences. Since a candidate function's associated orthogonal function is calculated by removing the common energy between it and previous functions, it is easy to see that in these cases the orthogonal function may have most of it's energy removed. As a result, $D(m,m)$ can become small and as a result of numerical precision on a computer, this can result in large values for g_m.

Most computer systems, in particular MATLAB, store decimal values using floating point arithmetic and have a limited precision with which they can store any value. As a result of this, two e□ects occur. The first e□ect is that any calculation that results in more digits than the precision of the system has the results truncated to the maximum the system can allow. The second e□ect is that the resolution of any calculation is limited to the smallest interval that the floating point precision can produce. In addition, when two small numbers are added or subtracted, the mantissa of the smaller number is shifted in order to align the decimal points of the two values. This can result in very few non-zero binary digits in the smaller number. Once the mathematical operation is complete, the mantissa is shifted to the left and and the exponent readjusted. If the two numbers were close in magnitude, only a few of the bits may be non-zero, resulting in numerical imprecision for small numbers.

These phenomenon can introduce error into the $D_{m,m}$ calculations, which in turn iteratively impact the implicit calculations of α_{mr}, g_m and MSE as the FOS algorithm progresses. The impacts are exacerbated as the values of

$D(m,m)$ decrease, if $D(m,m)$ is very small, large numerical errors can occur and when dividing by D(m,m) much larger results can be produced than are mathematically accurate. A limitation on the values which $D(m,m)$ can be allowed to take can reduce these e□ects. If a candidate function is selected for addition to the functional expansion based on it's Q value, but does not have a su□ciently high $D(m,m)$ it is rejected as a candidate and the next highest Q is selected. As with the other thresholds, the risk of setting the $D(m,m)$ threshold at too high a value is that the system may reject suitable candidates for which the e□ects of the limited system precision are less minor, and the final functional expansion will become less optimally fit. Various $D(m,m)$ thresholds were tested and it was found that $1 \quad 10^{\ 6}$, was su□cient to maximize the ability of the FOS algorithm to fit closely spaced candidate functions, while avoiding erroneous g_m values.

4.1.4 Fitting Candidates

If the variable Q is used to represent the product of the squares of any time average orthogonal function and its associated weight, that is:

$$\begin{aligned} Q &= g_m^2 \overline{w_m^2(n)} \\ &= g_m^2 D(m,m) \end{aligned} \tag{4.18}$$

then Q is actually a measure of the MSE reduction that results from adding the m^{th} term to the functional expansion. Therefore the candidate function for which the Q is largest is selected as the first fitted term for the functional expansion from equation Equation 4.1. This function is then removed from the list of available candidate functions, and the remaining MSE between the input signal and the fitted functions is decremented by Q.

The process is repeated to find the next candidate term. The candidate function which best fits the remaining MSE is added to the functional expansion. That is, the candidate with the highest Q value without overshooting the remaining MSE (as overshooting the remaining MSE would cause the expansion to have more energy that the original signal), is removed from the available candidates and the remaining MSE is recalculated. This is repeated until a predetermined stopping limit has been reached.

After reaching a stopping limit, the orthogonal weights can be converted back to the candidate functions and weights. Since the orthogonal functions have a unique correspondence to the candidate functions, converting back is trivial. However, the candidate function weights (a_m) must be calculated from

their corresponding orthogonal weights (g_m). The formula for this conversion is given by [33]:

$$a_m = \sum_{i=m}^{M} g_i v_i \tag{4.19}$$

where v_i is a weighted sum of the previously calculated GS orthogonal weights, e□ectively reversing the orthogonalization back to the original candidate function weights. This can be calculated by[33]:

$$\begin{aligned} v_m &= 1 \\ v_i &= \sum_{r=m}^{i\ \ 1} \alpha_{ir} v_r \qquad i = m+1, \ldots, M \end{aligned} \tag{4.20}$$

4.1.5 FOS Stopping Criteria

There are several possible criteria that FOS can use to determine its stopping point. One stopping point can be placed once a certain amount of the overall energy has been fitted. This can be accomplished by calculating the ratio of the remaining MSE compared to the input signal's variance and comparing this value to a pre-determined limit[33]. If the threshold has been met, the algorithm can be stopped before attempting to select another term.

Another approach or criterion can be applied when a candidate function is selected for addition to the functional expansion. If it is determined to be fitting no more energy than would be fitted by WGN then it can be assumed all the remaining energy is noise and the algorithm can be stopped [34]. To test this, it is first assumed that the remaining energy can be descried entirely by WGN. If this is the case, then the correlation coe□cient, r, between the remaining energy and the sum of the fitted orthogonal functions can be described by the formula

$$r = \left[\frac{Q(M)}{\overline{y^2(n)} \sum_{m=0}^{M\ \ 1} g_m^2 D(m,m)} \right]^{1/2} \tag{4.21}$$

Since it is assumed that the remaining energy is WGN, r is assumed to be normally distributed with a standard deviation of $\frac{1}{\sqrt{N+1}}$ where N is the sample size of the input time series [30]. Given this, r must follow the inequality

$$|r| < \frac{1.96}{\sqrt{N}} \tag{4.22}$$

with a probability of approximately 95% [30]. Equation 4.21 and Equation 4.22 can be combined and simplified to show that if

$$g_M^2 D(M,M) < \frac{4}{n}\left(\overline{y^2(n)} \quad \sum_{m=0}^{M\ 1} g_m^2 D(m,m)\right) \tag{4.23}$$

or

$$Q(M) < \frac{4}{n}(MSE) \tag{4.24}$$

then the current term to be fitted is not fitting more energy than would be fitted by WGN [30].

The third stopping criterion that can be given to the FOS algorithm is to limit the number of fitted terms. This check is performed at the same time as one would check the overall fitted energy. If the desired number of terms have been fitted, the FOS algorithm can be stopped. This was the chosen approach when using the FOS algorithm for data analysis in this thesis. A detailed explanation of why this methodology was chosen can be found in Chapter 6.

The fourth possible cause to stop the algorithm is when the list of candidate functions has been exhausted. If all the given candidate functions have been fitted to the functional expansion, there remains nothing for the algorithm to fit and it must therefore stop.

4.2 Spectral Analysis Using FOS

Spectral analysis on a sample signal can be conducted using the FOS by selecting candidate frequencies (f_m) as matched sine and cosine pairs at various frequencies according to the following formula [31]:

$$\begin{aligned} p_{2m\ \ 1}(n) &= \cos\left(\frac{2\pi f_m n}{N}\right) \\ p_{2m}(n) &= \sin\left(\frac{2\pi f_m n}{N}\right) \end{aligned} \tag{4.25}$$

The algorithm is modified to find the combined Q of the cosine/sine pair and use this as the basis for fitting the next term. The pair selected to be the next fitted term are then added to the functional expansion as the $2_m \ \ 1$ and 2_m terms, as shown in Equation 4.25.

Once the FOS algorithm has fitted the candidate frequencies, the matched sine and cosine pairs can be reconstituted into a single term with magnitude $F(f_m)$ and phase $\phi(f_m)$ given by [31]:

$$F(f_m) = \sqrt{a_{2m\ 1}^2 + a_{2m}^2} \tag{4.26}$$

$$\phi(f_m) = \tan^{\ 1}\left(\frac{a_{2m}}{a_{2m\ 1}}\right) \tag{4.27}$$

Candidate frequencies for spectral analysis using FOS are then selected as a collection of single frequency sinusoids where the frequencies of the candidates vary across the spectrum of the signal. Candidate frequencies that are fitted by this method represent the frequencies present in the spectral analysis with magnitude and phase given in Equation 4.26 and Equation 4.27.

Because the candidate functions are pre-determined and passed to the FOS algorithm, it is possible to vary the frequency resolution across the spectrum being analyzed by simply increasing or decreasing the frequency difference between different candidate functions. This allows the computational cost of spectral analysis to be reduced in frequency bands where high resolution is not necessary while maintaining higher resolution where it is desired. In the initial spectral analysis tests, the candidate frequencies were evenly spaced at 1Hz across the entire range of relevant frequencies. When it became necessary to increase the frequency resolution to 0.1Hz, the candidate frequency spacing was only reduced to 0.1Hz across those frequencies where multiple pieces of equipment had demonstrated energy. This is discussed in further detail in Subsection 6.4.2.

5 Experimental Data

5.1 BURNSi and UWN Trial Reports

In February and March of 2021, DRDC published two trial reports; the Orca Benchmark Underwater Radiated Noise Simulation (BURNSi) Measurement Trial [35] and the Orca Underwater Noise (UWN) Measurement Trial Report [36]. These reports detail a series of hydro-acoustic noise measurement trials that were conducted at the Canadian Navy's underwater sound range in Patricia Bay, near Sidney, British Columbia, that DRDC conducted for research on the impact of ship noise on marine life [35]. Both trials used patrol craft, training (PCT) Moose, a Canadian Orca class vessel and were conducted as a series of static and dynamic range 'runs'. The dynamic runs consisted of passes of the vessel between two hydrophones at a variety of ship speeds and with different arrangements of operating machinery. The static runs were conducted by anchoring the vessel between two hydrophones and shutting down the ship. Individual pieces of equipment were then run to collect the hydro-acoustic noise generated by that piece of equipment alone. The static runs also included several runs where artificial noise sources were recorded. These noise sources included a piezoelectric 'shaker' which is capable of producing a wide variety of tones within the ship as well as more transient noise sources such as popping balloons, hammer blows on the ship's machinery and piping, and tones played over a portable loudspeaker.

Both trial reports and the complete archive of the data collected during these trials were generously provided by DRDC for this thesis. As a result, there is a wealth and quality of data that would not have otherwise been available without a significant expense in both time and budget.

5.2 Patricia Bay Acoustic Range

The Patricia Bay acoustic range is a hydro-acoustic range owned and operated by the RCN. It is located near Sidney, British Columbia and is comprised of two discrete sound ranges, the Static Range and the Dynamic Range. The Static Range comprises two hydrophones situated 200m apart that rest 1m above the ocean floor on pedestals [37]. Due to the sloping bottom, the northern hydrophone rests 19m from the water's surface and the southern hydrophone sits 22m from the water's surface [37]. A four point mooring system is centred between the hydrophones in order to allow a ship to rest in a fixed position and allow the ship to shut down completely without drifting. The hydrophones in the Dynamic Range are situated 212m apart and are set on the same pedestals as the Static Range; the bottom slope at the dynamic range results in the north hydrophone resting 28m from the surface and the south hydrophone resting 44m from the surface [37].

5.3 Static and Dynamic Runs

5.3.1 Static Runs

Static Range runs were conducted in support of both the BURNSi and UWN measurement trials in July of 2019 and February of 2020, respectively [36][35]. During the BURNSi trial, the Static Range trials commenced with an ambient sound recording and followed with 24 runs focusing on the ship's diesel generators (DGs). The three DGs were recorded running in isolation and with other pieces of equipment added as significant noise sources. The intent by DRDC during these trials was to correlate the hydro-acoustic noise generated by the DGs with vibration data collected onboard PCT Moose[36]. Subsection 5.4.2 contains a discussion on the vibration readings taken using a data acquisition system (DAQ) fitted onboard the vessel. A list of the Static Range trials, with the DG that was used and additional equipment that was run can be found at Appendix A.

During the UWN trial, the intent was to collect acoustic data for the major pieces of machinery onboard [35]. DRDC conducted a series of runs, commencing with an ambient noise reading and then a run for each major piece of machinery. For each of these runs, the targeted piece of machinery was the only operating machinery (with the exception of hotel services such as lighting and electrical power to operate the machine) and the remainder of the ship was powered o. During these runs, the piezoelectric 'shaker' was also tested. It was installed directly on the ships hull framework and operated at pure 500Hz,

1 kHz, 2 kHz and 4 kHz tones. While normally static ranging is conducted with the ship at a four point mooring, as discussed in Section 5.2, due to personnel and time constraints this trial was conducted with the ship at anchor [35]. DRDC sta recognized in their report that this was not ideal and would result in small variations in the acoustic levels received by the hydrophones as a result of the ship swinging on its anchor chain, but they determined that the resulting data would still be su cient for any frequency analysis [35]. Table A.5 contains a list of the planned Static Range runs conducted as a part of the BURNSi trial. Cells indicated by yellow fill were unable to be completed due to machinery or other limitations, and are therefore unrepresented in the final hydrophone data. A list of the Static Range runs that were conducted for the BURNSi trials are located at Appendix A

5.3.2 Dynamic Runs

Dynamic sound range trials were conducted over a combined 5 days over the course of the UWN and BURNSi trials. The purpose of these trials was relatively straightforward, with the aim being to establish the general noise generated by the ship when travelling at a range of speeds from 3 to 20 knots. These trials were completed in pairs of runs, with the ship travelling in both directions (East and West) at every speed and machinery configuration. The planned track for the ship was directly in between the hydrophones and both the actual speed by Global Positioning System (GPS) and the distance of the planned track were recorded. Machinery states varied from the normal operating state to the various states enumerated in Figure A.1. Conducting each trial in both directions allows both hydrophones to record the resulting noise from both the Port and Starboard sides of the ship. This can help identify if any noise generated by the ship is highly directional (i.e. emits specifically from one side of the ship) and helps balance the e ect of the ships hull blocking radiated background noise from outside the range between the two sides of the ship as well. As with the Static range runs, a complete list of the applicable Dynamic range runs can be found at Appendix A.

5.3.3 Collection Methodology

In both the static and dynamic runs, the methodology of data collection was to maintain the systems on PCT Moose in a static configuration. On the static runs, systems were not turned on or o during recording and in the dynamic runs, the ship was travelling in a straight line at constant speed. While this met the needs of the DRDC trial, it does not represent a realistic

model of ship behaviour. Even as the ships are entering and leaving harbour, which was explained in Section 3.3 as the ideal time to collect EHM data for the application this thesis is exploring, it cannot be guaranteed that the ship will not maneuver or alter speed. If time and resources had permitted the collection of hydro-acoustic data for this research, more dynamic runs might have improved the realism of the results. Much of the machinery of interest in this research, however, is predominately stable in time. As was discussed in Section 2.1, mechanical noise tends to be independent of variations in ships speed. This means that the static nature of the DRDC trials does not significantly reduce the realism of the research. A second mitigating factor that allows the DRDC trial data to be useful and realistic for this research is the selection of the FOS algorithm as the feature selection or spectral analysis tool. As was discussed in Section 3.3, the FOS algorithm can perform spectral analysis on a significantly shorter sample than similar spectral analysis tools. These short samples allow the time-varying portions of the ship's radiated noise to be approximated as time invariant, by sampling them faster than the noise varies.

5.4 Collected Data

In addition to the hydro-acoustic noise gathered by the sound range, DRDC also collected the GPS data for each of PCT Moose's dynamic runs and collected onboard vibration data. Vibrometers were fitted at several locations in the machinery spaces and records were kept to coincide with the static and dynamic runs via a 20 channel data recorder [35].

5.4.1 Hydro-Acoustic Data

Audio data from the hydrophones at the Patricia Bay acoustic range was collected by the operating sta of the range and stored as a custom binary file with an encoding format that was developed by a subcontractor of Lloyd's Register Applied Technology, who were contracted to the Navy's Directorate of Naval Platform Systems.

Each Binary file begins with 10 bytes of header data. The first two bytes are a 16 bit integer that, if set to 0, indicate the underwater gain of the microphone was 20dB. Any other value in this space indicated a gain of 40dB was used. The remaining 8 bytes hold a flattened double-float string that indicates the maximum absolute voltage value contained in the file.

After the header data, each binary file contains a series of data elements. Each data element has its own header data, which consists of 16 bytes of data.

The first four bytes encode a status label which are either filled with blank spaces (i.e. an integer value of 32), or the special status "COM" to indicate the commencement of recording, "FIN" to indicate the completion of recording, and "CPA" to indicate closest point of approach. The fourth character in all three cases is a blank space. The next 4 bytes of data is a flattened 32-bit number that encodes the sequence number of the data element. This is used to identify missed data during a recording so it can be recovered and placed in sequence. All data provided by the range sta was complete without missing elements. The final component of the data header is a flattened 8 byte double-float that indicates the voltage range of the data acquisition card. This is for information only, as the data can be recovered without referring to this value.

Finally, each data element contains 1.5 seconds of raw audio data sampled at 204,800Hz, for a total of 307,200 individual samples. These raw samples were multiplied by 20,000,000 and converted to 32-bit flattened integers after recording, thus to convert back to original raw voltages the saved data must be converted back into a floating double and divided by 20,000,000. The minimum resolution of the data acquisition card used for this system is 1.25μV, which is converted to 25 when encoded into the binary file, thus the conversion is lossless. The sensitivity of the hydrophones installed on the Patricia Bay ranges are $2.24mV/Pa$. Form this, the data encoded in the binary file can be converted directly into a noise amplitude. Figure 5.1 shows how the custom file format is encoded.

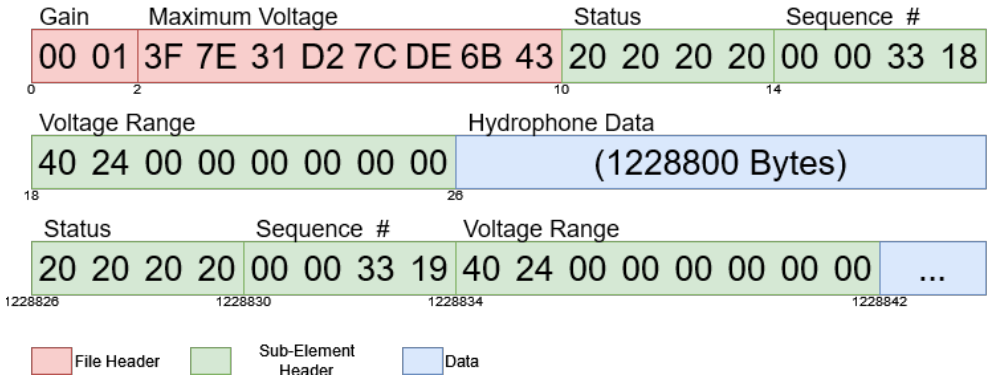

Figure 5.1: DRDC Custom Binary File Format

The hydro-acoustic data was also provided in a .wav format, which is a digital audio encoding format developed by Microsoft and IBM. This allows the data to be played by a standard computer media player, and MATLAB contains a native function to decode .wav files. Each sample in a .wav file

is saved as a 16-bit value. This results in a significant amount of data from the hydrophones being clipped at the maximum value when being saved as a .wav file. These clipped areas behave like a square wave when being spectrally analysed and generate a theoretically infinite number of harmonics of the base frequency that is being detected (as the Fourier expansion of a square wave is an infinite sum of the odd harmonic sinusoidal waves). The loss of data and the generation of non-existent harmonics renders the .wav files unsuitable for use in this application. Figure 5.2 shows a sample time series from a .wav file provided by DRDC, taken from the recording of PCT Moose's starboard diesel generator, with the resulting spectrogram. The harmonics can clearly be seen repeating at regular multiples of the fundamental frequency.

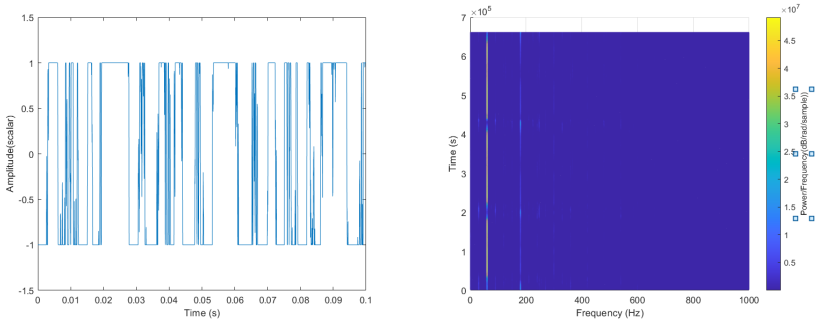

Figure 5.2: Example of .wav File Time Series and Resultant Spectrogram

5.4.2 Vibration Data

For both trials series, DRDC installed a DAQ on PCT Moose. This system was a multi channel array of accelerometers, tachometers, and rudder angle indicators. The tachometers were fitted to each of PCT Moose's two shafts and the rudder angle indicators were fitted to the rudders. The accelerometers were fitted to various pieces of equipment and moved throughout the trials to collect vibration data in accordance with the DRDC trial plan [38]. The DAQ was controlled by a computer which recorded the collected data with time-stamps so that the data could be aligned to the individual runs.

While the scope of this thesis did not include analysis of the internal vibrations, part of the DRDC trials was to investigate the transmission paths of vibrations and sounds through the structures of the ship to assess whether the ships radiated noise could be estimated from the internally measured vi-

brations, and leads to potential future examination. This is discussed in more detail in Chapter 8.

5.4.3 Other Data

In addition to the DAQ, the DRDC computer was also connected to a standalone GPS. This allowed the trials staff to compare the expected and actual speeds of the ship in case of discrepancy and to plot the ship's position as it travelled between the hydrophones for track errors. Additionally, the binary acoustic data provided by DRDC did not appear to have been populated with the status tags for run commencement, closest point of approach (CPA), and finish (see Subsection 5.4.1). It may be possible to use the GPS data to confirm where these markers should be in the data, but this was not undertaken. Ultimately the baseline assumptions about the effects of Doppler shift were not correct, and more sophisticated Doppler management would be required in order to apply the algorithms from this thesis in a dynamic setting. This is discussed in further detail in Section 6.7

6 Experimental Methodology

6.1 Baseline Investigations

In order to better understand the data and to confirm the baseline assumptions that the noise generated by the ship would have strong line spectra, the data provided by DRDC was first investigated using a spectrogram. As discussed in Chapter 2, it was expected that the sound data would display strong frequency responses that were clearly visible above any background noise as well as being stable in time. Figure 6.1 demonstrates the spectrogram, showing the sound intensity in dB across the frequency range from 0Hz to 1kHz over time of a single static range trial where the main fire pump was run. The figure shows clearly discernible lines at 60Hz and 180Hz where significant energy was detected. This energy also appears to be fixed at the detected frequency across the entire time of the trial, indicating that the baseline assumptions are reasonable.

It was also necessary to confirm the expectations that machinery noise remains a dominant component of ship radiated noise when the ship is moving at low speeds. Spectrograms of dynamic range trials for PCT Moose at 5 knots and 15 knots, were generated and compared. These spectrograms can be seen in Figure 6.2. These clearly demonstrate that prominent line spectra are visible at both speeds, but also include significant noise at increased speeds. This is in keeping with the expectation that propeller noise and hydrodynamic noise increase as a function of speed and are broadband in nature.

6.2 Data Selection

Due to the iterative nature of the FOS algorithm and the requirement for point-by-point correlations, the computational cost of performing spectral analysis increases greatly as the number of candidate frequencies and the sample size grow. As a result, it was necessary to limit the data to expedite the compu-

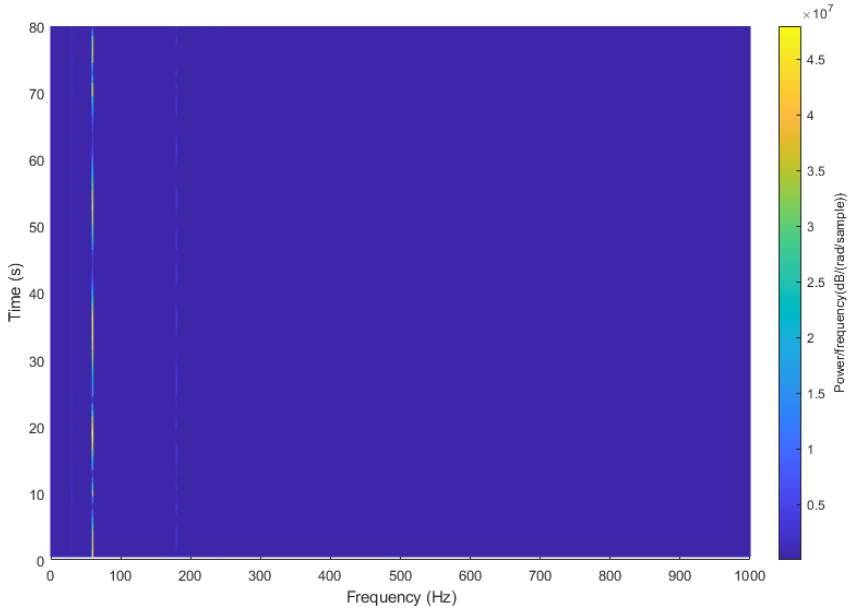

Figure 6.1: Static Range Spectrogram (in dB) of Fire Pump Operation

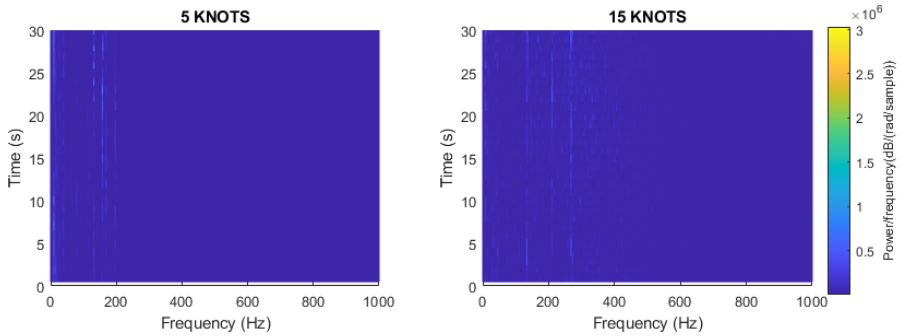

Figure 6.2: Noise Comparison (in dB) of PCT Moose at 5 Kts vs 15 Kts

tations carried out by the FOS algorithm. Since the maximum frequency of interest for this study was approximately 5kHz, it was possible to down-sample the data without negatively impacting the study results.

An analysis of the spectrograms produced by the static range trials for each piece of equipment that was individually recorded in the UWN trial showed that the majority of the sound energy produced by all the equipment occurred

below 2kHz, with the exception of the shaker which was specifically tested at 4kHz. This was supported by the DRDC reports, which concluded that noise levels from machinery decreased by approximately 30dB between 1kHz and 10kHz [36]. As a result of the relatively low sound levels at high frequencies, it was decided that the frequency of the acoustic data that was provided by DRDC could be down-sampled twenty times from the recorded rate of 204,800Hz to 10,240Hz. This sampling frequency would result in a Nyquist frequency of:

$$f_N = \frac{f_s}{2} = 5012Hz \tag{6.1}$$

where f_N is the Nyquist frequency; the maximum discernible frequency for a given sampling rate, f_s. Frequencies higher than the Nyquist rate will experience aliasing, a phenomenon where a signal appears to be of lower frequency due to it being under-sampled. To avoid this, the signals were down-sampled using the built-in decimate function in MATLAB. This function automatically applies a low pass filter to remove higher frequency signals when down-sampling. With a sampling rate of 10,240Hz, the computational cost of conducting spectral analysis using FOS was reduced to a more manageable size for experimentation by reducing the candidate frequency list and the sample size of the data, while maintaining the detectable frequency range high enough to detect energy at all relevant frequencies.

Another method to down-sample data can be achieved by the use of a moving average filter, where the average of the data to be removed in down-sampling becomes the new data point. This allows the partial preservation of some of the data being removed by the down-sampling and results in a more accurate representation of the original data in the down-sampled results. While it was not implemented for this thesis, the use of moving average based down-sampling techniques could improve the results of future research and should be considered.

6.3 Setting the FOS Parameters

Proper tuning of the FOS algorithm is critical to its correct functioning. This is achieved through the management of the stopping criteria of the algorithm, setting the $D(m, m)$ threshold to limit numerical instability, and by carefully selecting the candidate frequency list.

6.3.1 WGN Threshold

As described in Subsection 4.1.5, the WGN threshold is a mathematically derived threshold based on the MSE reduction caused by fitting WGN as the next term at a predetermined confidence interval. As was seen in Subsection 2.2.2, the background noise in hydro-acoustic environments cannot be expected to be white noise. Instead it is unpredictable, containing tones, broadband noise and harmonics based on background sources and their distance to the hydrophone. Without complex noise pre-processing it will not be possible to set a WGN threshold such that no background noise is inadvertently fitted without also risking that the threshold will be reached without fitting energy originating from the target system. In one experiment, for example, using the static range acoustic data for the 500Hz shaker, raising the WGN threshold caused the 500Hz tone to no longer be fitted. As a result, it was decided that modifying the WGN threshold would not be effective and the test derived in Subsection 4.1.5 was used without modification.

6.3.2 Fitted Energy Threshold

The fitted energy threshold indicates the percentage of the total energy that must be fitted before stopping the FOS algorithm. This value can be set to any level and choosing a higher threshold will result in a more accurate estimate for the input with a smaller residual error. Conversely, choosing a lower threshold will result in a higher residual error, but will result in fewer selected terms and quicker computation time. The FOS algorithm fits terms in descending order of energy fitted, therefore each newly fitted term represents incrementally less energy in the original signal than the previous. Due to the variable nature of the background noise, as well as the intent for a detection system that can detect equipment when the ship is at variable distances to the hydrophones, it is not possible to predict how much of a received signal is expected to be equipment noise and how much is expected to be background noise. As a result, a threshold value of 99% of the energy being fitted was set. As before, this would ensure that the algorithm would stop if the background noise in a given sample was particularly low, but in most cases it was expected that another threshold would stop the algorithm.

6.3.3 Number of Fitted Terms

The number of fitted terms threshold is an arbitrary limit that simply ends the algorithm after a user defined number of terms have been fitted. Fitting more terms necessarily means that more of the input signal's energy will be

captured by the algorithm, at the cost of increased computational time for each added term. While this compromise may sound similar to the one presented by the previous thresholds, it is subtly di□erent. In the previous approaches, the threshold limit was being placed on the amount of fitted energy. Since each fitted terms represents incrementally less total system energy, as the FOS algorithm fits more terms, the incremental change in fitted energy and resulting residual error decrease. As the number of fitted terms increases, the incremental changes in fitted energy becomes very small. At these small increments, slight changes to the previous thresholds can result in large and unpredictable changes in the number of fitted terms. Since each additional fitted term causes an increase in the computational time of the FOS algorithm, these changes can significantly a□ect the computational time for the algorithm to complete. By stopping the algorithm based on the number of fitted terms, it is possible to limit this e□ect, resulting in more predictable computational times. Given the experimental nature of this thesis, it was deemed that having a predictable computational cost and time would be beneficial and it was therefore decided that the primary limiting threshold for the algorithm would be the number of fitted terms.

Because the fitted terms threshold is not mathematically derived, the number of important terms was empirically derived. The FOS algorithm was run for spectral analysis on thirty 1s samples of the static range data for all the tested equipment as well as a sample of the range ambient noise from the same day. The number of fitted terms was varied from 10 to 200. As expected, the computation time rose dramatically with increased fitted terms. Figure 6.3 shows the processing time required for the FOS algorithm to spectrally analyze a single second of acoustic data, sampled at 10,240Hz, the sampling rate used for this study. It shows that the processing time for each iteration of the FOS algorithm is exponentially proportional to the number of fitted terms. At 200 fitted terms, the FOS algorithm required approximately 500s to complete one iteration. To complete the thirty iterations for one recorded system would therefore requires more than 4 hours.

Examining the results from these trials showed that the candidate function weights, p_m from Equation 4.1, and therefore the fitted energy, quickly diminished after the first few fitted terms. After the algorithm had fitted between 10 and 15 terms, the energy represented in new terms was similar to comparable terms fitted for the ambient noise data. As a result, these terms would be of little value in identifying characteristic features of any equipment. In order to ensure that variations in the equipment noise or background noise of untested samples would be captured, a safety margin was added to the number of fitted terms that was deemed useful for feature identification and 30 fitted terms was

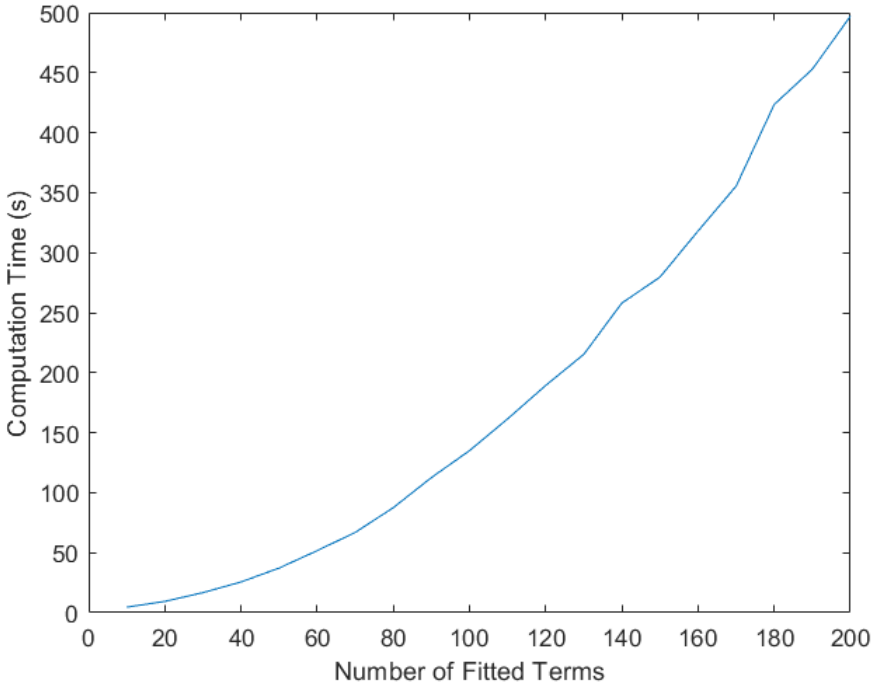

Figure 6.3: Processing Time for 1s of Acoustic Data at 10,240Hz Sampling Rate)

used for all the initial experiments to find the equipment features.

Thirty fitted terms was used for nearly all experiments to identify features and the subsequent classifier tests that resulted from those features. Based on Figure 6.3, it could be expected that the FOS algorithm would require approximately 30 seconds to complete calculations. This means that any classifier based on this implementation of the FOS algorithm would be incapable of processing acoustic data as it was collected, in real-time. As discussed in Section 3.3, one of the assumptions that led to the decision to use the FOS algorithm for this application was that it was not required to perform real-time analysis. Many current EHM techniques, such as vibration analysis or oil content analysis are not conducted in real-time, but rather over several days or weeks where samples are collected and sent to a specialist for analysis. In this respect, complete processing in the order of only a few minutes would be an improvement in EHM processing time. However, the possibility of improving

the speed of the classifiers to be capable of processing in real-time is worthy of investigation. Further discussion on how the acceleration of FOS and classifier calculations can be achieved are discussed in Section 3.3.

6.4 Generating the Acoustic Profile

Once the FOS algorithm's parameters were adequately set, the investigation of the acoustic profile of the ship commenced. The data used for this investigation was taken from the UWN trial data provided by DRDC. This data was broken into 26 individual recordings of equipment. Upon investigation, however, it was found that the recorded data for run number SRJ4PB23AX01XB (see Appendix A for a detailed explanation of run numbering conventions), which was the trial for the #1 fresh water pump, was corrupt and not usable. The recording for trial SRJ4PB23AX00XB contained the #1 fresh water pump operating with its hot water heater running concurrently. Similar recordings were made for the #2 fresh water pump and hot water heater. It was decided, therefore, to treat the fresh water pumps and their fresh water heaters a single system. Additionally, four of the recordings were taken with only the piezoelectric shaker running at different frequencies. These were also grouped into a single system. This resulted in 21 unique systems being spectrally analyzed in order to build the acoustic profile for PCT Moose.

6.4.1 Initial Spectral Analysis

The purpose of the initial spectral analysis was to identify the unique frequencies that each piece of equipment generated as part of its noise profile. For this, it was initially assumed that 1Hz frequency resolution would be sufficient to detect unique frequencies for each piece of equipment. If spectral analysis was being conducted using the FFT, 1Hz resolution would be calculated as $1/T$ where T is the sampling period, meaning that a 1s sample would be required. The frequency resolution of FOS is 10 times that of a similar FFT [8], therefore a 0.1s sample would be sufficient to achieve this resolution. The first thirty seconds of each UWN static range trial was therefore broken into 0.1s segments and spectral analysis was conducted on them using the parameters that had been determined in the previous sections. Using Equation 4.26 and Equation 4.27, the fitted cosine and sine pairs for each spectral analysis were converted into a single fitted frequency term and plotted into a single cluster plot. This plot displayed each fitted term for each system as a single point on a graph with the frequency and magnitude of the terms represented by the x and y axes, respectively. Each system was given a unique symbol to improve

legibility. The cluster plot is included at Figure 6.4. The plot was then manually inspected for locations where plotted points on a single location on the frequency axis were generated by only one piece of equipment.

During this investigation, two findings were observed. The first finding was that it was impossible to discern unique frequencies for all pieces of equipment at 1Hz frequency resolution. While some equipment did display unique frequencies that were readily identified, much of the machinery shared common frequencies with several other pieces of machinery. It became apparent from this that in order to identify all the equipment, either other techniques for feature identification would be required, or higher frequency resolution would be necessary to identify the differences between the individual components.

Table 6.1 contains a table of the equipment with unique frequencies identified during the initial spectral analysis. These frequencies were determined manually, by inspection of the cluster plot. It is important to note that while the shaker was recorded while set to produce 500Hz, 1kHz, 2kHz, and 4kHz tones, it appeared to be producing harmonics and sub-harmonics and was detected at many of the uniquely identified frequencies regardless of what frequency it was expected to be producing.

Table 6.1: Unique Frequencies Generated by PCT Moose Equipment

Equipment	Unique Frequency
Port Diesel Generator	442Hz
Centreline Diesel Generator	1064Hz, 1319Hz
Engine Room Fan	265Hz
Bilge Pump	51Hz, 454Hz
Fuel Pump	1151Hz, 1152Hz, 1153Hz, 1154Hz
Starboard Fuel Filter Set	1239Hz
Shaker	500Hz, 999Hz, 1000Hz, 1001Hz, 1999Hz 2000Hz, 2001Hz, 3999Hz, 4000Hz, 4001Hz

The second finding was that the starboard diesel generator was completely indiscernible in the clutter of the scatter plot. For every frequency that the generator had energy based on the spectral analysis, there was a plethora of other equipment that was also fit at a similar amplitude. After some investigation it was realized that this was due to the fact that the starboard diesel generator was likely running during the trial for every other piece of equipment in order to provide the electrical power for the ship and the system being recorded. While the trial report indicates that the port diesel generator is

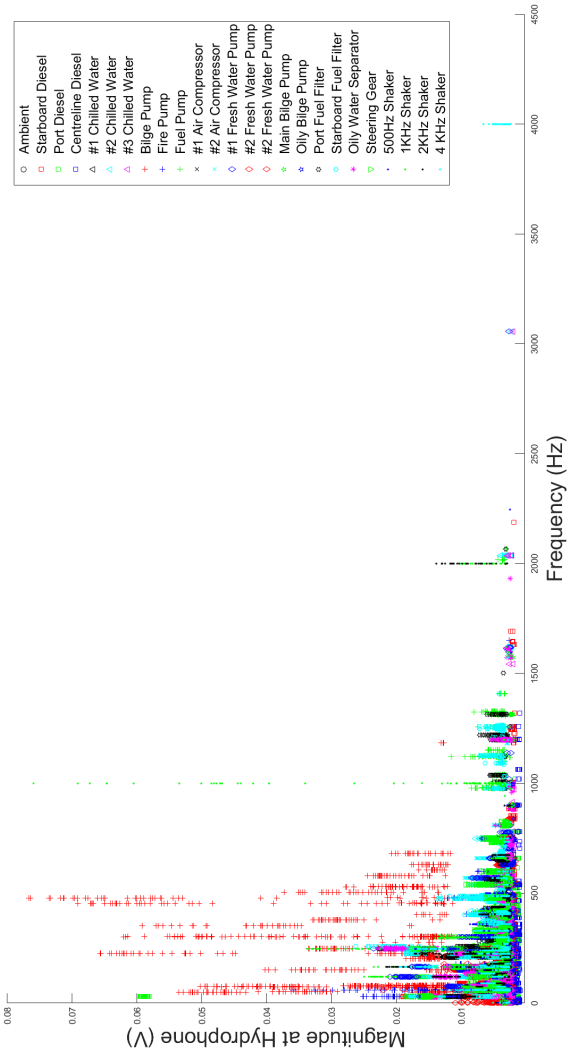

Figure 6.4: Cluster Plot Generated for Initial Spectral Analysis

normally the primary generator, the starboard diesel generator was recorded immediately prior to testing all the other systems (see Table A.1). It is reasonable to assume that the generator would not be changed before moving to the next trial in order to save time. This assumption became relevant in Subsection 6.5.1

It became infeasible, therefore, to discern a unique frequency for the starboard diesel generator purely by examining the fitted frequencies fitted for each system. There was no way to confirm if a frequency fitted for any of the other systems that matched those of the generator running in isolation were solely as a result of the generator running or whether that equipment was contributing some energy at that frequency as well.

6.4.2 Refined Candidate Frequency List

Based on the inability to identify unique frequencies for each of the systems at 1Hz resolution, and the congregation of many of the equipment frequencies around a few key frequencies, it was determined that spectral analysis on the static range system recordings should be re-conducted with a higher spectral resolution. This would require an increase in the sample length used for each spectral analysis to 1s in order to allow for the FOS spectral resolution to be 0.1Hz. The UWN static range trials collected acoustic data for between 93s and 94.5s for each piece of equipment, therefore 300 samples would no longer be possible, as was used in Subsection 6.4.1. Instead, 90s of data was used as this allowed the maximum amount of data to be analyzed while maintaining the same data size for each piece of equipment.

In order to optimize the FOS algorithm the candidate frequencies selected for for spectral analysis were not chosen to be uniformly spaced at 0.1Hz. Instead, 1Hz spacing was maintained except across those frequencies where there was a concentration of data points, indicating several pieces of equipment had fitted energy at that frequency.

A new unique frequency table was developed from the results of this investigation using the same methods as in Subsection 6.4.1. The increased frequency resolution at frequencies of interest resulted in an expanded feature list and helped to identify some instances where two pieces of similar equipment shared a unique frequency. The chilled water plants, for example, all contained detected energy at 33.8Hz. This makes sense, since the three systems are redundant systems and would therefore be nearly identical. As a result, in the cases where frequencies were unique to a set of redundant systems, a new feature was established as an identifier that one of these redundant systems was running, though which system specific system had not been iden-

tified. The refined unique frequency table from this investigation are presented in Table 6.2.

Table 6.2: Refined Unique Frequencies Generated by PCT Moose Equipment

Equipment	Unique Frequency
Port Diesel Generator	442Hz
Centreline Diesel Generator	1064Hz, 1319Hz
Any Chilled Water System	33.8Hz
#3 Chilled Water System	26Hz
Engine Room Fan	265Hz
Bilge Pump	51Hz, 454Hz
Fuel Pump	1151Hz, 1152Hz, 1153Hz, 1154Hz
Any Fuel Filter Set	460Hz, 461Hz, 462Hz
Port Fuel Filter Set	1037Hz
Starboard Fuel Filter Set	1239Hz
Shaker	500Hz, 999Hz, 1000Hz, 1001Hz, 1999Hz 2000Hz, 2001Hz, 3999Hz, 4000Hz, 4001Hz

6.4.3 Initial Detection Tests

Using the frequencies identified via the training data, a classifier was built. This classifier takes the results of the spectral analysis performed by FOS, examines the list of fitted frequencies and compares it to the list of feature frequencies from Table 6.1. Detection of any of the systems is a simple binary decision based on whether the feature frequency had been fit in the spectral analysis.

In Subsection 6.4.2, it was discussed that the training data used for building the feature sets were 90 second samples from each piece of equipment's UWN static range trial. Since each recording was between 93s and 94.5s long, there was between 3 and 4.5 seconds of additional hydro-acoustic data for each system. This data was ideal for initial testing as it was not used for training, but had been collected during the same experimental conditions meaning environmental conditions would be unlikely to a□ect the results of the detection test.

A test set of hydro-acoustic data was therefore built using the final 3 seconds of recorded data for each system as well as the final 3 second of the ambient data, for a total of 75s of hydro-acoustic data. The data was sampled

at 1s intervals and the classifier was run on those samples for each of the 7 systems with features identified in at Table 6.1. The candidate frequencies given to the FOS algorithm were spaced at 1Hz and spanned the range from 1Hz to 5120Hz, and the used stopping threshold was 30 fitted terms. Table 6.3 contains the results of this initial trial, presented as a confusion matrix.

Table 6.3: Confusion Matrix Results from Initial Detection Trial

		Estimated Status	
	Total 30+495=525	Running	Not Running
Actual Status	Running	21	9
	Not Running	2	493

Taking each of the 7 features being classified as a single test and multiplying by the seventy-five 1s intervals yields a total of 525 unique tests. Table 6.3 shows that the classifier was correct in identifying the presence or absence of a system 514 times and incorrect 11 times. There is a probability of detection of 70%, a probability of false detection of 0.4% and a total probability of error of 2.1%.

Following the successful operation of the classifier, and the high accuracy of the initial feature set in detecting the presence of running machinery, further testing was conducted. The classifier was expanded to include the new features identified in Table 6.2. The classifier experiment was then re-conducted using the refined candidate frequency list as the FOS candidate frequencies and 50 fitted terms, as it is expected that the increased frequency resolution would require more fitted terms to accurately analyze.

The second detection trial retained the seventy-five 1s samples of the initial trial, but the feature set was expanded to 11 terms, representing the 11 systems being classified, resulting in a total of 825 individual tests. The confusion matrix for this trial is displayed in Table 6.4. On this trial, the classifier achieved a probability detection of 76%, a probability of false detection of 4.6% and total probability of error rose to 5.8%. The probability of false detection had the greatest increase between the two trials, exhibiting an twelve-fold increase in the second detection trial.

To understand the cause for this increased rate of error, the results of the second trial were broken into two subsets; the results generated by the original 7 features, and those generated by the 4 new features. It was found that the false positive rate within the new features for this trial were one third that of the original feature set. This implies that the new feature set was working correctly, however, the increased number of fitted terms had raised

Table 6.4: Confusion Matrix Results from Second Detection Trial

		Estimated Status	
	Total 50+775=825	Running	Not Running
Actual Status	Running	38	12
	Not Running	36	739

the error rate in the original terms. As elaborated in Section 6.3, the number of fitted terms served as the stopping criterion to achieve a balance between the accuracy of spectral analysis and the level of background noise that the FOS algorithm fits to the functional expansion. The increase in fitted terms to allow the second trial to better identify the new features, had apparently cause more noise to be fitted, greatly increasing the error rate overall.

To confirm this diagnosis, the trial was re-conducted. This third trial used the same setup as the second trial, with the exception that the FOS algorithm was restricted to the same 30 term limit as in the initial trial. As Table 6.5 shows, the probability detection for this trial was 68%, the probability of false detection was 0.8% and total probability of error was 2.8%, which is similar to the results from the initial trial.

Table 6.5: Confusion Matrix Results from Third Detection Trial

		Estimated Status	
	Total 50+775=825	Running	Not Running
Actual Status	Running	33	17
	Not Running	6	769

6.4.4 Comparison with the Fourier Transform

In order to evaluate the performance of the classifiers developed using the FOS algorithm, a classifier was built that uses the FFT as a base for feature extraction. This classifier conducted an FFT on the seventy-five 1s segments of test data from the initial detection trial. The resulting spectral analysis had a frequency resolution of 1Hz, therefore it could be compared against the initial detection trial results. The spectral analysis was then analyzed and all the local maxima were found. These local maxima represented the best estimates of the component frequencies of the recording by the FFT. The local maxima were then compared to the feature frequencies identified in Table 6.1. If a local

maximum was at the same frequency as the feature frequency, the classifier assessed the system as 'running.' The confusion matrix results for the FFT based classifier can be seen at Table 6.6. The probability detection for the FFT based classifier was 96.6%, which seems at first to be much more effective than the FOS based classifier. Looking further, however, the FFT classifier demonstrated a probability of false detection of 61.4% and total probability of error was 58.1%, demonstrating much poorer performance overall. The reason for this is likely due to the FFT analyzing all the energy available in the sample, including the ambient noise. In order to improve the results of the FFT based classifier, the recorded data would need to be pre-processed to remove ambient noise. Further comparisons between an FFT based classifier and the developed FOS based classifiers are not possible. The remaining classifiers require a frequency resolution of 0.1Hz, which would require test segments 10s long to analyze via the FFT. Since the available test data for each system is only 3s long, there is simply not enough data for the FFT to achieve the required resolution. From this we can conclude that the FOS based classifiers are functioning very well. They have demonstrated an ability to classify systems using very short data samples and in the presence of ambient noise levels that rendered a similar classifier using the FFT ineffective.

Table 6.6: Confusion Matrix Results from FFT Trial

		Estimated Status	
	Total 30+495=525	Running	Not Running
Actual Status	Running	29	1
	Not Running	304	191

6.5 Second Order Features

Following the successful implementation of simple feature selection and its ability to precisely predict the operational state of the equipment onboard PCT Moose, a new trial was conducted. This trial aimed to determine if a more complex feature could be identified and used as a basis for a classifier. For this trial, the same cluster plot from Subsection 6.4.1 was used. The plot was manually searched for instances where the spectrogram for an individual system demonstrated clustering at two frequencies based on the following criteria:

1. Over the 90 individual spectral analyses, both frequencies must have been fit greater than 80% of the time, and

2. Both frequencies may be fit for any number of systems, but the clusters for the system of interest must be at unique amplitudes relative to the other systems at that frequency

Three systems were found that matched these criteria, port diesel generator, starboard diesel generator and the #1 chilled water plant. Table 6.7 contains the frequency pairs as well as their associated normalized mean and standard deviation.

The experimental conditions and environmental conditions during the static range recordings make it impossible to guarantee that the noise levels received at the hydrophones for each system would be representative of future noise levels for those systems. Slight variations in the ships distance to the hydrophone, the temperature, salinity of the water and myriad other conditions can all impact the received noise levels. However, it is expected that the relative relationships among individual line spectra for any system should not be significantly a□ected by environmental conditions. That is, if a system emits two tones, f_1 and f_2 at a relative noise level ratio of 2:1 during the static range recordings, this ratio will also be demonstrated for the frequencies in future recordings.

To exploit this expected relationship between the frequency pairs, it is necessary to assume that the variability in the magnitudes assigned for each of the frequencies in the feature pair for each sample were e□ectively randomly generated. Since we assume that the controllable experimental conditions (distance to the hydrophones, system setup, etc.) didn't change greatly across the various samples, then it is fair to assume the variations in received energy are due to uncontrollable and unpredictable environmental issues and assigning a random nature is reasonable. As a result, it is also reasonable to assume that the distribution of the magnitudes calculated by the FOS algorithm across the static range samples will follow a normal distribution, and the variability of the fitted magnitudes can be described by their mean value and standard deviation. Since what is actually necessary to describe is the behaviour of one frequency to another, it is necessary to first normalize the fitted magnitude of the frequency pairs against each other. This is achieved by dividing the magnitude assigned for both frequencies by the sum of the magnitudes of both frequencies. This gives a ratio for both frequencies that sums to 1. Computing these values for each of the 90 samples (or each of the samples for which both frequencies were fitted by the FOS algorithm) gives two sets of normalized magnitude values. From these values a mean and standard deviation can be extracted.

A classifier was then built to capitalize on these relationships. This was

Table 6.7: Second Order Feature Frequency Pairs

Equipment	Frequency Pair	Normalized Sample Mean	Normalized Standard Deviation
Port Diesel Generator	30Hz, 45Hz	.94, .06	.044, .044
Starboard Diesel Generator	90Hz, 195Hz	.70, .30	.05, .05
#1 Chilled Water System	33.8Hz, 105Hz	.70, .30	.05, .05

achieved by use of the z-score, which is a statistical measure calculated via the formula[39]:

$$z = \frac{x \quad \overline{x}}{S} \tag{6.2}$$

where x is the value of an individual sample, $\overline{x}$ is the sample mean and S is the sample standard deviation. It is important to note that $\overline{x}$ and S are closely related to μ and σ. The difference is that μ and σ describe the mean and standard deviation of the entire population. Sample mean instead describes the observed mean, given by the formula [39]:

$$\overline{x} = \frac{\sum_{n=1}^{N} x_n}{N} \tag{6.3}$$

where x_n are the individual samples and N is the total number of samples taken. Sample standard deviation is calculated as [39]:

$$S = \sqrt{\frac{\sum_{n=1}^{N} (x_n \quad \overline{x})^2}{N \quad 1}} \tag{6.4}$$

The sampled data represents a small subset of the total population of possible samples, thus $\overline{x}$ and S are assumed to be approximations of the true mean and standard deviation. As sample size increases, it can be assumed that sampled mean and standard deviation will converge to the true mean and standard deviation.

By Equation 6.2, we can see that the z-score is simply a calculation of the number of standard deviations a single measurement is from the sample mean. A confidence interval is a range where a set of measurements can be expected to occur and is typically measured as a number of standard deviations from

the sample mean. One standard deviation about the mean results in a confidence interval of approximately 68%, and two standard deviations results in a confidence interval of approximately 95%, where the percentage represents the number of samples of a population will appear within that interval [39]. The frequency pair classifier was designed to take the magnitudes fitted by the FOS algorithm for identified frequencies, normalize them against each other and compute a z-score using the mean and standard deviation derived from the training data. The z-score was then compared to a variable threshold number of standard deviations. If both normalized magnitudes fell within the prescribed number of deviations from their respective means, then the relationship between the two frequencies was assumed to be the same as that seen during the analysis of the training data for that system and the system was predicted to be running. This allowed a variable stringency to be applied to the classifier. A larger confidence interval would increase the likelihood of the classifier predicting a feature is present when the two feature frequencies were detected. This increases the likelihood of detection, but also the likelihood of false detection. Conversely, a smaller confidence interval decreases the likelihoods of detection and false detection by requiring the sample values to be nearer to the sample means.

It is also important to note that this classifier requires both feature frequencies to have been identified by the FOS algorithm for fitting to the functional expansion. The absence of either frequency would cause the classifier to predict the system was not running. Although this might appear to suggest that the classifier is less prone to generate false negatives initially, it must also be considered that the frequencies being selected for these features were not unique to each piece of equipment, meaning the frequencies were generally more likely to be present, even if the target system is not running.

Using the same 75s testing data as the previous experiments, the frequency pair classifier was tested twice. For this fourth detection trial, the previous classifiers were not used, and the z-score threshold was set to 1 standard deviation for the first test and 2 for the second.

6.5.1 Results of Second Order Feature Tests

When the z-score threshold was set to 1 standard deviation, the classifier accurately predicted the port diesel generator and starboard diesel generator when they were running in isolation and failed to identify the #1 chilled water plant when it was running. Increasing the z-threshold to two standard deviations enabled the classifier to correctly predict all three systems when they were running. However, in both cases the classifier was not able to detect the star-

board diesel generator running concurrently with any other equipment. If the assumption that it was the generator for all other trials (except for the other diesel generators) is true, this means that both classifiers had a false negative rate of approximately 84%. In both test cases, there were no false positive results.

Table 6.8: Confusion Matrix Results from Second Order Feature Tests

		Estimated Status	
	Total 72+153=225	Running	Not Running
Actual Status	Running	12	60
	Not Running	0	153

6.6 Testing the Classifiers over Time

To gauge the ability of the various classifiers to continue to detect features over time, a trial was conducted using all 14 feature sets previously identified and the same FOS algorithm settings as before. The test data was taken from the BURNSi trial static range data, which can be reviewed at Table A.5. While the DRDC report lists 24 individual trials, the recording were actually collected in groups of 3, and no recordings of run numbers SRF3PB02DE00XB, SRF3PB02DE01XB, SRF3PB02DE02XB were available. This resulted in 7 acoustic recordings, with a total length of 645s of recorded data. A summary of the results can be seen in Table 6.9

Table 6.9: Classifier Results from the BURNSi Trial

		Estimated Status	
	Total 826+8204=9030	Running	Not Running
Actual Status	Running	103	723
	Not Running	565	7639

After approximately 6 months elapsed time, the performance of predictions by the classifier appeared to have degraded severely. Reviewing the individual results for each sample second and each feature leads to some possible reasons why this has occurred. Analysis of this data shows that the classifier was almost perfectly accurate when predicting based on the feature identified for the bilge pump. During the 88 seconds it was running, it was predicted to

be running for all 88 samples. The vast majority of the errors from this trial, both false positive and false negative, are driven by the classifier identifying the wrong diesel generator as running and failing to identify the correct one. After some investigation, the cause for the failure to identify any diesel generator was identified. Five second samples of each of the systems or pairs of systems was analyzed via the fast Fourier transform and the average FFT spectrogram was overlaid on a similar length sample of the ambient noise recording taken on the day of the trial. Figure 6.5 shows the resulting graphs and it can be seen that for all but trial number SRF3PB03LI, the trial where the bilge pump was run concurrently with the centreline diesel generator, the recorded sound is nearly identical in spectrum to the ambient conditions. It is not clear whether these recordings are correct representations of the change to the ships noise signature or whether there was some issue transcribing the files when the data was recorded. It is evident from the spectrograms that there is minimal energy available at the feature frequencies for the diesel generators, as confirmed by the classifier.

For comparison, Figure 6.6 shows a 5 second averaged spectrogram of the port diesel generator and the ambient noise recorded during the UWN trials. This figure clearly shows several tones exhibited by the generator that are not present in the background noise, including its 442Hz feature tone. Figure 6.5 shows that any modification to the FOS algorithm that would allow enough terms to fit the feature frequencies (if they were fit at all) would also cause more background noise tones to be fit, increasing false positive rates up.

The spectrogram for trial number SRF3PB03LI shows significant energy at a variety of frequencies not exhibited in the ambient noise. During this trial, the centreline diesel generator and bilge pump were running. Recalling that the classifier correctly identified the presence of the bilge pump in every sample of this trial, it can be concluded that, while the generators may have changed in their acoustic profile in the interim time between the UWN and BURNSi trials, the bilge pump remained similar enough between trials to allow it to be detected again.

6.7 Dynamic Range Test

The final experiment conducted for this research was to implement the full classifier suite on samples of hydro-acoustic data taken from the dynamic range portion of the UWN trial. It is necessary, therefore, to examine the effect of a ship's movement on the perceived radiated noise via the Doppler shift.

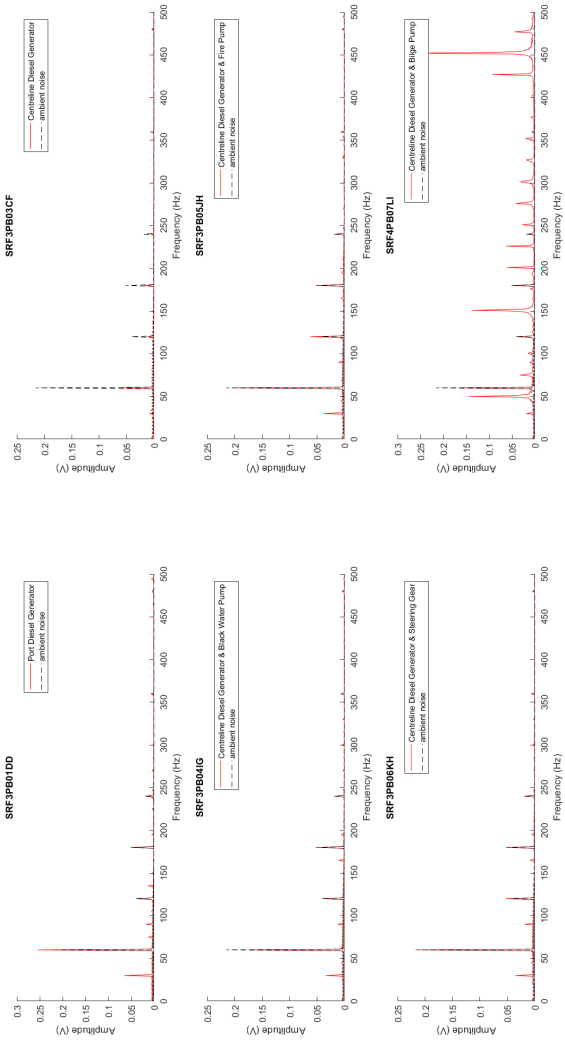

Figure 6.5: Spectrograms of BURNSi Trial Data

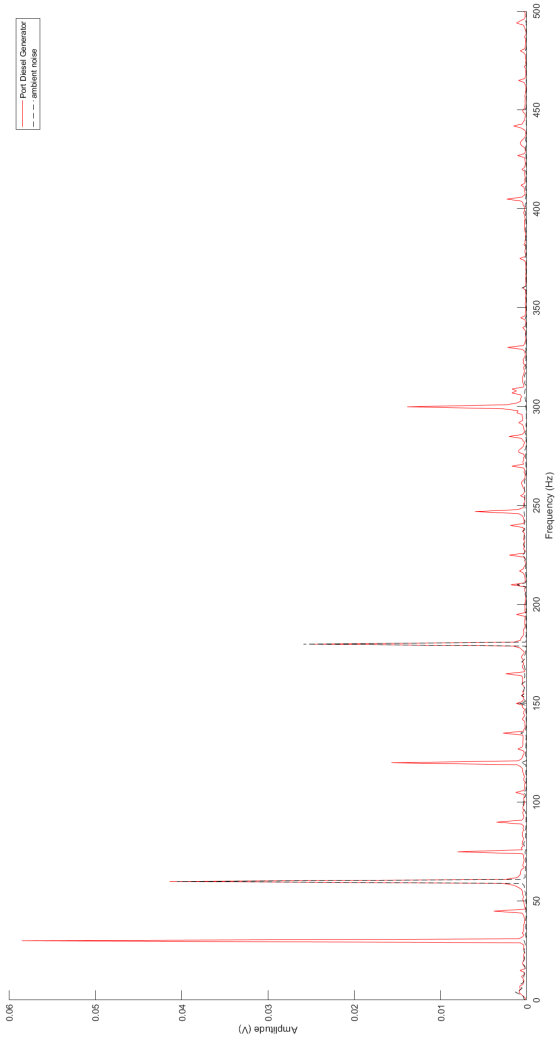

Figure 6.6: Spectrograms of UWN Port Diesel Generator and Ambient Noise

6.7.1 Doppler Shift

The general formula for Doppler shift for a moving source and a stationary observer is [40]:

$$f_o = \frac{f_s}{1 \quad \frac{v_s \cos\theta}{c}} \tag{6.5}$$

where f_o is the frequency perceived by the observer, f_s is the frequency emitted by the source, v_s is the speed of travel of the source, θ is the angle of travel of the source relative to the perceived direction of the wave arriving at the observer (i.e. 0°would be a source travelling directly toward the observer) and c is the speed of wave transmission in the given medium. E□ectively, this formula states that the frequency received by a stationary observer is a□ected by the speed and direction of travel of the source and the e□ect is more pronounced as the speed of the source increases relative to the speed of wave transmission in the medium. The formula also shows that the Doppler e□ect results essentially in a ratio multiplier of the source frequency, thus higher frequencies experience greater frequency shifts than lower frequencies.

In order to gauge the overall e□ect of Doppler on an experiment like those performed by DRDC, a similar experiment can be simulated. A noise source emitting a range of frequencies can be moved past a stationary observer and the resulting Doppler shifts calculated. The speed of sound selected for this experiment was $1500\frac{m}{s}$, as this was approximately the maximum speed of sound measured by DRDC during the UWN trial, and a maximum speed of sound term will result in maximum Doppler shift values. Figure 6.7 shows the resulting Doppler shift across a range of frequencies as a source moving at 5 knots (2.57 $\frac{m}{s}$).

This graph demonstrates that Doppler shift is significant at very shallow approach angles and at broader angles quickly recedes, becoming zero as the approach angle to the hydrophone reaches 90°, as would be expected. Also, as expected, lower frequencies are significantly less a□ected by Doppler Shift than higher frequencies. We can see that emitted frequencies below 500Hz do not shift more than 1Hz, regardless of approach angle. Increasing or decreasing the speed of the noise source causes a commensurate change in the Doppler shift values, without changing the sinusoidal shape of the data.

6.7.2 Dynamic Range Test Results

Since a main advantage of the FOS algorithm is its improved frequency resolution, even at very short sample intervals, a 1s sample was taken from the centre of trial numbers DRJ1PB05AX00EB, DRJ1PB05BX00EB, DRJ2PB05CX00EB,

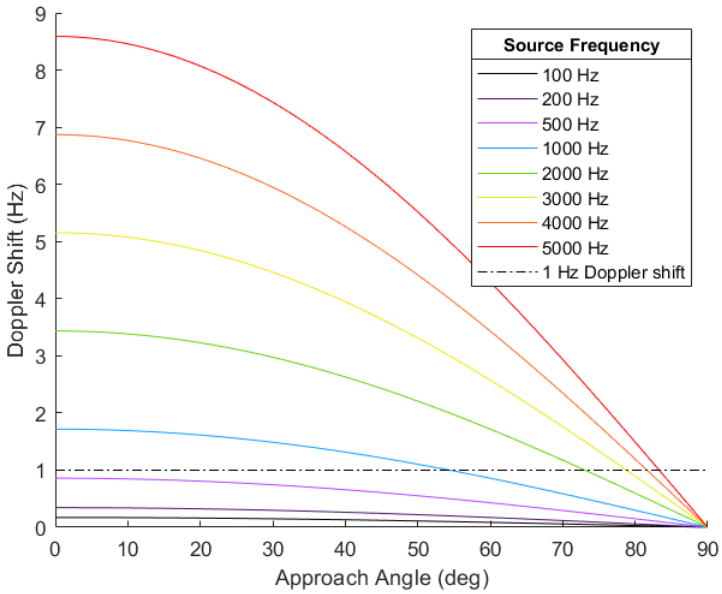

Figure 6.7: Doppler Shift for 5Kt Moving Source

DRJ2PB05DX00EB, DRJ2PB05EX00EB, DRJ2PB05EX00EB, DRJ2PB05FX00EB, DRJ2PB05GX00EB, and DRJ2PB05GX00EB. These trials constitute a representative sample of the UWN static range trials where PCT Moose was travelling at 5 kts. By selecting from the centre of the recordings, it was ensured that the vessel was at or near CPA, meaning that the Doppler shift was expected to be minimal or zero. Selecting only one second of data ensured that the vessel's approach angle did not progress significantly past 90°, while still providing enough data for the FOS algorithm to achieve the necessary frequency resolution for feature detection.

Testing the complete set of classifier feature on this data resulted in the algorithm failing to estimate that any systems were running, representing a complete failure of the classifier. A second test was conducted, using the entire recording of run number DRJ2PB05FX00EB. In this dynamic run, the bilge pump was cycled on and o periodically as the vessel travelled past the hydrophone. Since the bilge pump was successfully identified in all previous trials, it was reasoned that it would be the most likely to be successfully identified again. The classifier failed to estimate that the bilge pump was running across the entire recording.

Two possible causes for the failure of the classifier are that the addition of the main propulsion equipment caused significant changes to the acoustic signature of PCT Moose, and that the assumptions about Doppler shift were incorrect. During the static range trials, the main engines were not recorded. When they were operated for the dynamic trials, it is possible that their acoustic signature was loud enough to e□ectively drown out the other systems. Figure 6.8 shows the acoustic signature of PCT Moose during run number DRJ2PB05FX00EB. Several line spectrum components that were routinely visible in the static range recordings, such as the tones at approximately 60Hz, 120Hz and 180Hz remain visible here, suggesting that the addition of propulsion machinery acoustic signature did not significantly overpower the other machinery.

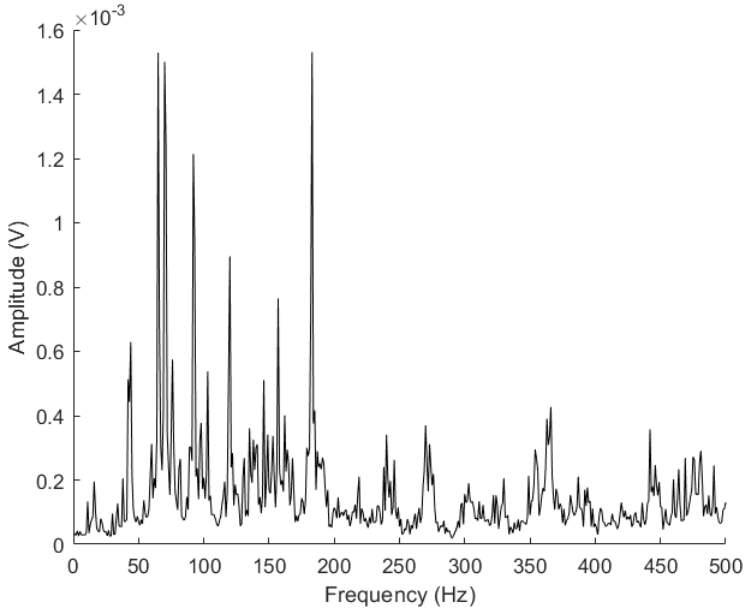

Figure 6.8: Acoustic Signature of PCT Moose Travelling at 5Kts

The assumptions about Doppler shift that were used during these research activities failed to take into account that, while the Doppler shift may minimal when PCT Moose is travelling perpendicular to the hydrophone, the rate of change of Doppler shift is conversely maximal. As a result, the frequencies being analysed are not static during the sample period, causing the FOS algorithm to fit di□erent frequency terms. In order to progress towards the

use of FOS on dynamic hydroacoustic data for EHM, it will be necessary to manage this effect by processing the data to account for Doppler shift. This is discussed in further detail in Chapter 8.

7 Conclusions

The goal of this thesis was to use the FOS algorithm on SRN in order to identify discrete pieces of equipment from samples of the ships radiated noise. Once the ability to identify equipment was established, The ability to detect the same equipment over long period of time and the ability to track the equipment as a ship moves was tested in order to establish the viability of using the FOS algorithm as a tool for monitoring a ship's equipment health. From these experiments, the value of continued research in the aim of producing a SRN based equipment health monitoring system using the FOS algorithm was determined.

The initial detection trials, utilizing only a single feature for every system, was shown to be highly capable of identifying some systems and predicting their presence in repeated trials. This ability was limited to those systems that had unique tones in their spectra, which was found in 7 of the 21 possible systems. Increasing the frequency resolution allowed for more unique frequencies to be identified. Further increased frequency resolution may be able to identify more features in this way, however, there was not enough data to support increased frequency resolution. The conclusion that can be drawn from this is that high frequency resolution techniques, in particular the FOS algorithm show promise in application to SRN for use in EHM. The results from this experiment strongly support continued research with greater data collection and at higher frequency resolutions.

Increasing the complexity of the features used for system identification, and using the relationship between the amplitude of two frequencies also showed promise at identifying equipment when the system was running in isolation. once the systems were running in conjunction with other systems (such as in the case of the diesel generators), the relationship between these frequencies did not appear to be the same. From this, it can be concluded that it appears possible to use higher order relationships within each system's noise profile as a basis for system identification, but more data and more sophisticated data analysis techniques would be required in order to confirm this.

The ability of the detection algorithms to continue detecting systems over time was tested, but the tests were largely unsuccessful. Among the systems tested in this experiment, the classifier showed to be very successful in identifying the bilge pump, but due either to changes in the acoustic profile of the diesel generators, their interactions with other systems, or some other issues, the classifier was not able to reliably detect the diesel generators. On the success of the classifier in detecting the bilge pump, it can be said that the stability of the acoustic profile of at least some systems over time seems likely and recommends further research in this area.

8 Future Work

The use of high resolution spectral analysis has been shown in this thesis to have promise in its application to SRN for the detection of shipboard equipment and the monitoring of that equipment over time for evidence of defects. There remains, however, much work that must be done in order to produce a working model of a system capable of identifying and tracking all of a ship's equipment and identifying defects. The following sections outline some areas of future work that have been identified for advancing this research beyond what has been achieved here.

8.1 FOS Variations

Since it's introduction, the FOS algorithm has had a number of variations developed that seek to improve its performance. In particular, it has been found that FOS can be sub-optimal [41][34]. By selecting the highest MSE reducing term at each step, and not revisiting that selection, the FOS algorithm inherently ignores the possibility that a combination of other terms may provide a better fit for the system. One improvement on the basic FOS algorithm is the fast orthogonal search with first term re-selection (FOS-FTR) [34]. In FOS-FTR, the FOS algorithm is initially run as normal. If the algorithm has fitted N terms, it is then re-run $N \quad 1$ times, each time force fitting a di□erent term from the original fitted terms (i.e. $n = 2 \ldots N$) as the first term, and re-selecting all the following terms as in normal FOS. This results in N total system estimations of the original input series, and the estimation that most reduces the MSE can be selected as the best representation of the true nature of the input series [34].

Another FOS variation that is similar to FOS-FTR, is an algorithm known as iterative fast orthogonal search (IFOS) [41]. Like FOS-FTR, IFOS begins by estimating the input series in the same way as the basic FOS algorithm. Where FOS-FTR kept a single term and varied all the remaining terms to seek

a better fit, IFOS instead de-selects only a single fitted candidate function, keeping all the rest fixed and selecting a new replacement for the deselected term in order to minimise MSE [41]. This is done for all the terms originally fitted, or until the MSE stops being reduced.

Both FOS-FTR and IFOS are improvements on the basic FOS algorithm. They have both been shown to more effectively reduce the MSE of the fitted model, and therefore provide a more accurate estimation of the input time series [34]. Since the primary method of identifying features in this thesis was based on spectral analysis, the increased accuracy provided by these methods may allow better identification of feature frequencies. Re-conducting this experiment using either of these methods and comparing the success rate of a system based on the original FOS algorithm and it's improvements would make a natural next step of progression to a complete defect identification system.

8.2 Expanded Sample Data

While the results for this thesis were encouraging, there were several shortfalls that the data set created that could be improved. The presumed use of the starboard diesel generator for all the static range trials that formed the basis of the training data caused significant issues in determining a feature for that diesel. In addition, since no piece of equipment was run concurrently with any other in the training data, there was no way to identify relationships between the various pieces of equipment that may become apparent when they are run together.

The UWN report comments that extensive sound ranging exercises similar to what was performed for PCT Moose are normally only conducted on military vessels and the results are classified [36]. As a result, detailed acoustic data for ships is rare. The results from this thesis make a strong argument for a significantly expanded experiment, collecting more data from each piece of equipment, as well as a variety of combinations of equipment.

8.3 Feature Selection

As was seen in Chapter 6, the feature selection techniques used in this thesis were based on unique frequencies, or the relationship between two frequency pairs, based on the assumption that they would vary in a predictable and coordinated manner. While this was effective in proving the concept of using high resolution spectral analysis as the basis for equipment identification and

monitoring from ship radiated noise, there is significant room to explore feature selection techniques for this application.

This would be especially true if coupled with a larger experiment. Trials conducted with varying subsets of the equipment, as opposed to single elements running in isolation might allow previously unnoticed relationships between the equipment to be detected. As the data set gets more complex, however, it will become impossible to manually inspect. Data analysis techniques such as principle component analysis (PCA), or machine learning techniques would be required to identify features.

8.4 Data Pre-processing

The results of the classifier depended heavily on the amount of noise that the FOS algorithm was allowed to fit in its functional expansion. This was managed by varying the number of fitted terms that the FOS algorithm used as its stopping criteria. There is a large body of research dedicated to managing hydro-acoustic noise. Pre-processing the recorded noise from this or further experiments in order to reduce the impact of ambient noise could conceivably allow the application of other stopping thresholds, such as the WGN or fitted energy thresholds, which could then be determined in advance of testing, likely improving the accuracy and the general applicability of future classifiers.

Additionally, processing the acoustic data to remove ambient noise would lead to shorter calculation times. By removing the ambient noise, there is less information contained in the input time series for the FOS algorithm to estimate. This would allow the algorithm to complete with fewer fitted terms which, as demonstrated in Subsection 6.3.3 has a direct impact on the processing time of the FOS algorithm.

Finally, selecting the data at moments when the ship was travelling directly perpendicular to the angle of transmission of its sound to the hydrophone was insu□cient to limit the e□ects of Doppler shift. This rendered the classifiers incapable of detecting any equipment when the ship was moving. The implementation of Doppler shift processing as part of the data pre-processing would therefore be an excellent subject for future work. This would enable the classifier to be used as originally envisioned, with the ship entering or leaving harbour and travelling past a hydrophone installed at the harbour entrance.

8.5 Parallel Computing

Improvements in data processing technology have made the processing of large amounts of data more expedient than ever before. In Subsection 6.3.3 it was shown that the computation time for the FOS algorithm increases in a square relationship with the number of fitted terms, and thus limiting the number of fitted terms allowed faster computation of the spectral analysis. Another method to increase the speed of spectral analysis would be to employ parallel computing. In parallel computing, the computational load of a calculation or series of calculations is spread between multiple processors. This could be achieved by conducting successive iterations of the FOS algorithm in parallel with each other. An example of this would be the spectral analysis of the training data, where successive segments of the recordings could be analyzed concurrently. This could also be achieved by identifying portions of the algorithm itself that can be calculated in parallel, thus reducing its processing time. This would allow much faster data processing and enable future research in this application to be conducted more quickly. If the algorithm were improved sufficiently, it could also lead to an application of a FOS based classifier capable of monitoring SRN in real time.

References

[1] F. Fahy and J. Walker, *Fundamentals of Noise and Vibration*. Taylor & Francis, 1998, isbn: 9780419241805.

[2] R. J. Urick, *Principles of Underwater Sound*. McGraw-Hill, 1975, isbn: 9780070660861.

[3] Y. Li, F. Ning, X. Jiang, and Y. Yi, "Feature extraction of ship radiation signals based on wavelet packet decomposition and energy entropy," *Mathematical Problems in Engineering*, vol. 2022, 2022.

[4] R. Li, W. Bu, and J. Cheng, "Research on ship-radiated noise evaluation and experiment based on otpa optimized by operation clustering," in *2021 OES China Ocean Acoustics (COA)*, IEEE, 2021, pp. 450–455.

[5] H. Yang, L.-l. Li, G.-h. Li, and Q.-r. Guan, "A novel feature extraction method for ship-radiated noise," *Defence Technology*, vol. 18, no. 4, pp. 604–617, 2022.

[6] *Canadian Forces Technical Order C-03-005-033/AA-000, "Naval Engineering Manual"*. 2012.

[7] *Canadian Forces Technical Order C-03-010-106/NW-007, "Vibration Analysis Applicable to Halifax Class"*. 2015.

[8] D. R. McGaughey, V. Dagenais, and S. P. Pecknold, "Improved torpedo range estimation using the fast orthogonal search," *IEEE Journal of Oceanic Engineering*, vol. 35, no. 3, pp. 595–602, 2010.

[9] C. Peng, L. Yang, X. Jiang, and Y. Song, "Design of a ship radiated noise model and its application to feature extraction based on winger's higher-order spectrum," in *2019 IEEE 4th Advanced Information Technology, Electronic and Automation Control Conference (IAEAC)*, IEEE, vol. 1, 2019, pp. 582–587.

[10] Y. Liu, Y. Lv, T. Lv, Y. Wei, and X. Liu, "Simulation of ship-radiated noise based on shallow marine environment," in *2019 IEEE International Conference on Signal, Information and Data Processing (ICSIDP)*, IEEE, 2019, pp. 1–5.

[11] Z. M. Hussain, A. Z. Sadik, and P. O'Shea, *Digital Signal Processing: An Introduction with MATLAB and Applications*. Springer, 2011.

[12] T. Fawcett, "An introduction to ROC analysis," *Pattern Recognition Letters*, vol. 27, no. 8, pp. 861–874, 2006.

[13] M. Farrokhrooz and M. Karimi, "Marine vessels acoustic radiated noise classification in passive sonar using probabilistic neural network and spectral features," *Intelligent Automation & Soft Computing*, vol. 17, no. 3, pp. 369–383, 2011.

[14] G. Li, Y. Hou, and H. Yang, "A novel method for frequency feature extraction of ship radiated noise based on variational mode decomposition, double coupled du□ng chaotic oscillator and multivariate multiscale dispersion entropy," *Alexandria Engineering Journal*, vol. 61, no. 8, pp. 6329–6347, 2022.

[15] Y. Li, Y. Li, X. Chen, and J. Yu, "A novel feature extraction method for ship-radiated noise based on variational mode decomposition and multi-scale permutation entropy," *Entropy*, vol. 19, no. 7, 2017.

[16] A. N. Akansu, W. A. Serdijn, and I. W. Selesnick, "Emerging applications of wavelets: A review," *Physical communication*, vol. 3, no. 1, pp. 1–18, 2010.

[17] N. E. Huang, Z. Shen, S. R. Long, *et al.*, "The empirical mode decomposition and the hilbert spectrum for nonlinear and non-stationary time series analysis," *Proceedings of the Royal Society of London. Series A: mathematical, physical and engineering sciences*, vol. 454, no. 1971, pp. 903–995, 1998.

[18] J.-R. Yeh, J.-S. Shieh, and N. E. Huang, "Complementary ensemble empirical mode decomposition: A novel noise enhanced data analysis method," *Advances in adaptive data analysis*, vol. 2, no. 02, pp. 135–156, 2010.

[19] M. E. Torres, M. A. Colominas, G. Schlotthauer, and P. Flandrin, "A complete ensemble empirical mode decomposition with adaptive noise," in *2011 IEEE international conference on acoustics, speech and signal processing (ICASSP)*, IEEE, 2011, pp. 4144–4147.

[20] Z. Chen, Y. Li, R. Cao, W. Ali, J. Yu, and H. Liang, "A new feature extraction method for ship-radiated noise based on improved CEEMDAN, normalized mutual information and multiscale improved permutation entropy," *Entropy*, vol. 21, no. 6, p. 624, 2019.

[21] K. Dragomiretskiy and D. Zosso, "Variational mode decomposition," *IEEE Transactions on Signal Processing*, vol. 62, no. 3, pp. 531–544, 2014.

[22] Y. Li, Y. Li, X. Chen, and J. Yu, "A novel feature extraction method for ship-radiated noise based on variational mode decomposition and multi-scale permutation entropy," *Entropy*, vol. 19, no. 7, p. 342, 2017.

[23] C. Bandt and B. Pompe, "Permutation entropy: A natural complexity measure for time series," *Physical review letters*, vol. 88, no. 17, p. 174 102, 2002.

[24] B. Fadlallah, B. Chen, A. Keil, and J. Principe, "Weighted-permutation entropy: A complexity measure for time series incorporating amplitude information," *Physical Review E*, vol. 87, no. 2, p. 022 911, 2013.

[25] M. Rostaghi and H. Azami, "Dispersion entropy: A measure for time-series analysis," *IEEE Signal Processing Letters*, vol. 23, no. 5, pp. 610–614, 2016.

[26] C. Bandt, "A new kind of permutation entropy used to classify sleep stages from invisible EEG microstructure," *Entropy*, vol. 19, no. 5, p. 197, 2017.

[27] Y. Li, X. Gao, and L. Wang, "Reverse dispersion entropy: A new complexity measure for sensor signal," *Sensors*, vol. 19, no. 23, p. 5203, 2019.

[28] S. Nandi, H. A. Toliyat, and X. Li, "Condition monitoring and fault diagnosis of electrical motors—a review," *IEEE transactions on energy conversion*, vol. 20, no. 4, pp. 719–729, 2005.

[29] G. King, M. Tarbouchi, and D. McGaughey, "Rotor fault detection in induction motors using the fast orthogonal search algorithm," in *2010 IEEE International Symposium on Industrial Electronics*, IEEE, 2010, pp. 2621–2625.

[30] M. J. Korenberg, "Fast orthogonal algorithms for nonlinear system identification and time-series analysis," in *Advanced methods of physiological system modeling*, Springer, 1989, pp. 165–177.

[31] D. R. McGaughey, M. Tarbouchi, K. Nutt, and A. Chikhani, "Speed sensorless estimation of AC induction motors using the fast orthogonal search algorithm," *IEEE Transactions on energy conversion*, vol. 21, no. 1, pp. 112–120, 2006.

[32] K. M.J. and P. L.D., "Applications of fast orthogonal search: Time-series analysis and resolution of signals in noise," *Annals of Biomedical Engineering*, vol. 17, no. 3, pp. 219–231, 1989, issn: 0025-326X.

[33] K. M.J., "A robust orthogonal algorithm for system identification and time-series analysis," *Biological Cybernetics*, vol. 60, no. 4, pp. 267–276, 1989.

[34] M. D.R., K. M.J., and A. K.M., "Using the fast orthogonal search with first term reselection to find subharmonic terms in spectral analysis," *Annals of Biomedical Engineering*, vol. 31, no. 6, pp. 741–751, 2003.

[35] L. Gilroy, "Orca benchmark underwater noise sumulation (BURNSi) measurement trial report," Defence Research and Development Canada, 2021.

[36] L. Gilroy, "Orca underwater noise measurement trial report," Defence Research and Development Canada, 2021.

[37] L. Gilroy, "Ship noise management and the orca class of ships," *Marine Pollution Bulletin*, vol. 174, pp. 113–196, 2022.

[38] L. Gilroy, "Orca underwater noise measurement trial plan," Defence Research and Development Canada, 2020.

[39] E. Kreyszig, *Advanced Engineering Mathematics*. Wiley, 1993.

[40] A. French, *Vibrations and Waves*. CRC Press, 2001.

[41] K. M.J. and A. K.M., "Iterative fast orthogonal search for modeling by a sum of exponentials or sinusoids," *Annals of Biomedical Engineering*, vol. 26, no. 2, pp. 315–327, 1998.

Appendices

A The Orca Underwater Noise Measurement and BURNSi Trials

The Orca UWN Measurement and BURNSi trials were conducted over several days in July of 2019 and February of 2020 and were seperate, but closely related trials [35]. The collected data included over 200 planned individual data collections ('runs') with several different categories of variable that could be altered between each run. As a result, DRDC developed a naming convention that would allow each run to be uniquely named, while simultaneously describing the run's experimental conditions. This naming convention consists of a fourteen character alpha-numeric code, where each character, or pair of characters encodes a descriptor of a run variable. Figure A.1 shows how the alphanumeric code is broken down into the run details.

The DRDC naming convention begins with a descriptor of the type of trial that was conducted [36][35]:

a) Balloon - the ship was moored on the Static Range and balloons were popped within the machinery space to evaluate the machinery space echo and sound transmission;
b) Dynamic Ranging - conducted on the Dynamic Range, the ship was required to pass between the north and south hydrophones for acoustic measurement;
c) Impact Test - the ship was moored on the Static Range and various pieces of machinery were struck with hammers of different size and material to determine the sound and vibration transmission characteristics of the equipment and mounts in the machinery spaces;
d) Shaker - the ship was moored on the Static Range and a piezoelectric noisemaker (known as the 'shaker') was attached in several locations in

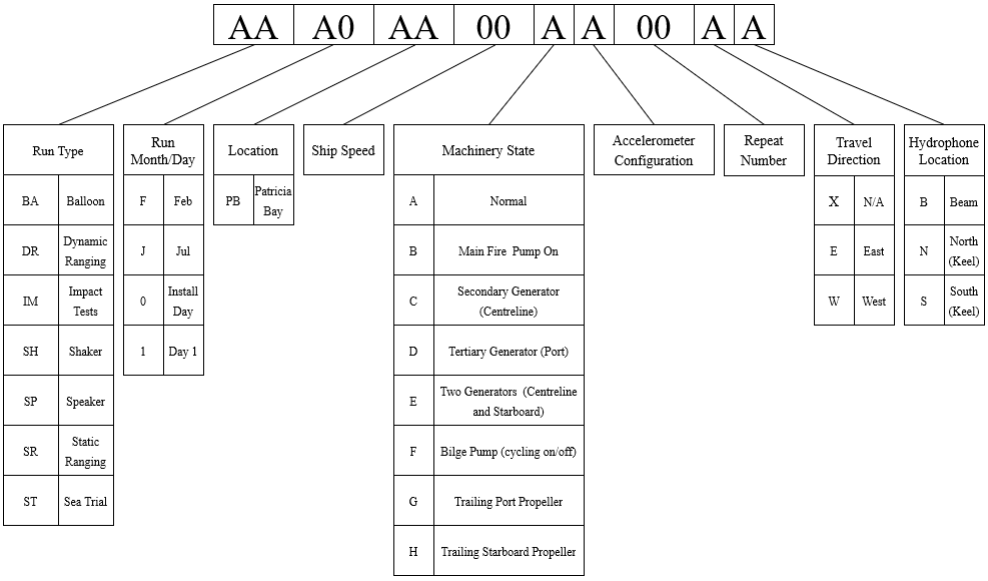

Figure A.1: DRDC Identifier Naming Convention

the machinery spaces. The radiated noise of the shaker was recorded. The shaker was set to produce individual tones and sweeping sine-waves;

e) Speaker - the ship was moored on the Static Range and a portable loud-speaker broadcast tones and swept sine-waves. The resulting radiated noise was recorded.
f) Static Ranging - the ship was moored on the Static Range and individual pieces of the ships machinery were run. All other equipment was o with the exception of electrical power and hotel services (e.g. lighting); and
g) Sea Trial - The ship conducted runs on the dynamic range focusing on the changes in vibration within the machinery room. There was no requirement during these trials for concurrent acoustic recording.

The second pair of characters are an alphanumeric set that indicate the month and day of the trial. The first digit encodes the month and the second encodes the trial day, with 0 representing the installation day. Subsequent days are sequentially numbered. The location identifier is given by two letters. These trials were all conducted at the Patricia Bay facility, which is represented by the code ‘PB’. Run speed is identified in the naming convention as a 2 digit number and represents the planned speed of the vessel, in knots. For Static Range runs, where the speed of the vessel is 0, the ship speed identifier is replaced with a simple consecutive numbering sequence. Each number

represents a specific Static Range trial (i.e. a specific piece of machinery or combination of machinery being recorded). The Machinery state identifies the predefined machinery configurations that DRDC intended to use during the trials. Machinery state A represents the normal machinery configuration for PCT Moose, and subsequent codes represent deviations from that normal state (e.g. adding a pump or running a secondary generator). Accelerometer configuration identifies the layout of the acceleromoter probe locations used in conjunction with the 20 channel DAQ. These locations are detailed in the DRDC reports [36][35]. The repeat number section of the identifier separates multiple instances of the same trial. The first time a run is conducted, it is considered repeat number 0, with each successive repetition of the same trial being incrementally numbered. The penultimate character of the naming system indicates the direction of travel of the ship across the range. On the dynamic range, the hydrophones are aligned in a North-South orientation, therefore the options of travel for the ship are East and West. An X indicates a stationary ship, as in the case of trials on the Static Range. The final digit in the system identifies which hydrophone was used. In almost all cases the ship was equidistant between both hydrophones and both hydrophones recorded the ship's beam aspect, as indicated by a 'B'. In some trials, however, the ship passed directly over the top of one of the hydrophones, in order to record the keel noise. This is indicated by the compass direction of the hydrophone that was passed over, North or South.

Although, as previously stated, there were over 200 runs conducted, the most relevant trial to this thesis were the Static and Dynamic trials. These trials contained the necessary data to form the acoustic profile, as well as the necessary recordings on which to conduct defect detection testing. As a result, the following tables detail only the Static and Dynamic Range trials that were conducted during the UWN and BURNSi trials [36][35]. Table entry items highlighted in yellow were not available, either due to failed recording at the range, or machinery considerations limiting the ability of the ship to conduct the run.

While the naming convention makes the identification of an individual run and its objectives unambiguous, reading the codes for runs can be difficult, especially if several codes are presented together. As a result, while the codes will be used in the main body of the thesis, they will normally be accompanied by a brief explanation of the specifics of the runs.

Table A.1: UWN Trial Static Range Runs

Run Number	Machinery Tested
SRJ4PB02AX00XB	Port DG
SRJ4PB03AX00XB	Centre DG
SRJ4PB04AX00XB	Stbd DG
SRJ4PB05AX00XB	Main Fire Pump
SRJ4PB06AX00XB	Emergency Fire Pump
SRJ4PB07AX00XB	Fuel Oil Transfer Pump
SRJ4PB08AX00XB	Port Fuel Filter Coalescer
SRJ4PB09AX00XB	Starboard Fuel Filter Coalescer
N/A	Air Conditioning Salt Water Cooling Pump
SRJ4PB11AX00XB	#1 Air Conditioning Condenser
SRJ4PB12AX00XB	#2 Air Conditioning Condenser
SRJ4PB13AX00XB	#3 Air Conditioning Condenser
SRJ4PB14AX00XB	#1 Air Compressor
SRJ4PB15AX00XB	#2 Air Compressor
N/A	Grey Water Pressure Pump
N/A	Sanitary Water Pressure Set
SRJ4PB18AX00XB	Oily Water Separator
N/A	Lubricating Oil Filling Pump
SRJ4PB20AX00XB	Main Bilge Pump
SRJ4PB21AX00XB	Oily Pilge Pump
SRJ4PB22AX00XB	Steering Gear Hydraulic System
N/A	Steering Gear Hydraulic Upper Power Pack
N/A	Steering Gear Hydraulic Upper Power Pack
SRJ4PB23AX00XB	#1 Fresh Water Pump with Hot Water Pump
SRJ4PB24AX00XB	#2 Fresh Water Pump with Hot Water Pump
SRJ4PB23AX01XB	#1 Fresh Water Pump
SRJ4PB24AX01XB	#2 Fresh Water Pump
N/A	Hot Water Pump
N/A	Black water pump #1—Not feasible
N/A	Black water pump #2—Not feasible
SRJ4PB28AX00XB	Engine Room Cooling Fan
SHJ4PB01AX00XB	500Hz Shaker
SHJ4PB02AX00XB	1 kHz Shaker
SHJ4PB03AX00XB	2 kHz Shaker
SHJ4PB04AX00XB	4 kHz Shaker

Table A.2: UWN Trial Dynamic Range Runs - Day 1

DRDC Identifier	Ship Speed	Machinery State	Direction	Track Error (m)
DRJ1PB03AX00EB	3	A	E	10
DRJ1PB03AX00WB	3	A	W	0
DRJ1PB03AX00EB	3	A	E	3
DRJ1PB03AX00WB	3	A	W	-2
DRJ1PB05AX00EB	5	A	E	2
DRJ1PB05AX00WB	5	A	W	4
DRJ1PB07AX00EB	7	A	E	2
DRJ1PB07AX00WB	7	A	W	-7
DRJ1PB09AX00EB	9	A	E	2
DRJ1PB09AX00WB	9	A	W	-1
DRJ1PB11AX00EB	11	A	E	-2
DRJ1PB11AX00WB	11	A	W	-2
DRJ1PB13AX00EB	13	A	E	10
DRJ1PB13AX00WB	13	A	W	-3
DRJ1PB15AX00EB	15	A	E	6
DRJ1PB15AX00WB	15	A	W	-10
DRJ1PB17AX00EB	17	A	E	2
DRJ1PB17AX00WB	17	A	W	-8
DRJ1PB17AX00EB	17	A	E	1
DRJ1PB13AX00WB	13	A	W	-2
DRJ1PB19AX00EB	19	A	E	-11
DRJ1PB19AX00WB	19	A	W	-10
DRJ1PB20AX00EB	20	A	E	-0
DRJ1PB20AX00WB	20	A	W	-7
DRJ1PB05BX00EB	5	A	E	-4
DRJ1PB05BX00WB	5	A	W	1
DRJ1PB11BX00EB	11	A	E	3
DRJ1PB11BX00WB	11	A	W	0

Table A.3: UWN Trial Dynamic Range Runs - Day 2

DRDC Identifier	Ship Speed	Machinery State	Direction	Track Error (m)
DRJ2PB05CX00EB	5	C	E	7
DRJ2PB05CX00WB	5	C	W	-3
DRJ2PB05DX00EB	5	D	E	8
DRJ2PB05DX00WB	5	D	W	0
DRJ2PB05EX00EB	5	E	E	2
DRJ2PB05EX00WB	5	E	W	1
DRJ2PB10EX00EB	10	E	E	10
DRJ2PB10EX00WB	10	E	W	-1
DRJ2PB15EX00EB	15	E	E	9
DRJ2PB15EX00WB	15	E	W	-7
DRJ2PB05FX00EB	5	F	E	-3
DRJ2PB05FX00WB	5	F	W	0
DRJ2PB05GX00EB	5	G	E	9
DRJ2PB05GX00WB	5	G	W	5
DRJ2PB05HX00EB	5	H	E	-2
DRJ2PB05HX00EB	5	H	W	5
DRJ2PB03AX01EB	3	A	E	-3
DRJ2PB03AX01WB	3	A	W	3
DRJ2PB05AX01EB	5	A	E	-2
DRJ2PB05AX01WB	5	A	W	-5
DRJ2PB09AX01EB	9	A	E	6
DRJ2PB09AX01WB	9	A	W	2
DRJ2PB11AX01EB	11	A	E	3
DRJ2PB11AX01WB	11	A	W	-4

Table A.4: UWN Trial Dynamic Range Runs - Day 3

DRDC Identifier	Ship Speed	Machinery State	Direction	Track Error (m)
DRJ3PB17AX01EB	17	A	E	5
DRJ3PB17AX01WB	17	A	W	-6
DRJ3PB19AX01EB	19	A	E	4
DRJ3PB19AX01WB	19	A	W	-13
DRJ3PB05AX02EB	5	A	E	0
DRJ3PB05AX02WB	5	A	W	-2
DRJ3PB05AX03EB	5	A	E	4
DRJ3PB05AX03WB	5	A	W	8
DRJ3PB09AX01EB	9	A	E	5
DRJ3PB09AX01WB	9	A	W	7
DRJ3PB09AX02EB	9	A	E	10
DRJ3PB09AX02WB	9	A	W	2
DRJ3PB19AX03EB	19	A	E	5
DRJ3PB19AX02WB	19	A	W	-6
DRJ3PB05AX00EN	5	A	E	Keel
DRJ3PB05AX00WN	5	A	W	Keel
DRJ3PB10AX00EN	10	A	E	Keel
DRJ3PB10AX00WN	10	A	W	Keel
DRJ3PB07AX01EB	7	A	E	-2
DRJ3PB07AX01WB	7	A	W	4
DRJ3PB08AX00EB	8	A	E	3
DRJ3PB08AX00WB	8	A	W	2
DRJ3PB08AX01EB	8	A	E	9
DRJ3PB08AX01WB	8	A	W	-2

Table A.5: BURNSi Trial Static Range Runs

DRDC Identifier	Diesel Generator	Additional Equipment
SRF3PB01DD00XB	Port	nil
SRF3PB01DD01XB	Port	nil
SRF3PB01DD02XB	Port	nil
SRF3PB02DE00XB	Port	nil
SRF3PB02DE01XB	Port	nil
SRF3PB02DE02XB	Port	nil
SRF3PB03CF00XB	Centreline	nil
SRF3PB03CF01XB	Centreline	nil
SRF3PB03CF02XB	Centreline	nil
SRF3PB04IG00XB	Centreline	Black Water Pump
SRF3PB04IG01XB	Centreline	Black Water Pump
SRF3PB04IG02XB	Centreline	Black Water Pump
SRF3PB04CG03XB	Centreline	nil
SRF3PB04CG04XB	Centreline	nil
SRF3PB04CG05XB	Centreline	nil
SRF3PB05JH00XB	Centreline	Main Fire Pump
SRF3PB05JH01XB	Centreline	Main Fire Pump
SRF3PB05JH02XB	Centreline	Main Fire Pump
SRF3PB06KH00XB	Centreline	Steering Gear
SRF3PB06KH01XB	Centreline	Steering Gear
SRF3PB06KH02XB	Centreline	Steering Gear
SRF4PB07LI00XB	Centreline	Emergency Fire Pump
SRF4PB07LI01XB	Centreline	Emergency Fire Pump
SRF4PB07LI02XB	Centreline	Emergency Fire Pump

Table A.6: BURNSi Trial Dynamic Range Runs - Day 1

DRDC Identifier	Ship Speed	Machinery State	Direction	Track Error (m)
DRF1PB03AA00WB	3	A	W	4
DRF1PB03AA00EB	3	A	E	N/A
DRF1PB05AA00WB	5	A	W	1
DRF1PB05AA00EB	5	A	E	9
DRF1PB07AA00WB	7	A	W	5
DRF1PB07AA00EB	7	A	E	4
DRF1PB09AA00WB	9	A	W	1
DRF1PB09AA00EB	9	A	E	3
DRF1PB11AA00WB	11	A	W	5
DRF1PB11AA00EB	11	A	E	2
N/A	13	A	W	6
DRF1PB13AA00EB	13	A	E	10
DRF1PB15AA00WB	15	A	W	2
DRF1PB15AA00EB	15	A	E	4
N/A	17	A	W	10
N/A	17	A	E	10
DRF1PB19AA00WB	19	A	W	15
DRF1PB19AA00EB	19	A	E	9
DRF1PB17AA01WB	17	A	W	15
DRF1PB17AA01EB	17	A	E	6
DRF1PB13AA01WB	13	B	W	4
	3	B	E	N/A

Table A.7: BURNSi Trial Dynamic Range Runs - Day 2

DRDC Identifier	Ship Speed	Machinery State	Direction	Track Error (m)
DRF2PB03AA00WB	3	A	W	3
DRF2PB03AA00EB	3	A	E	7
DRF2PB05AA00WB	5	A	W	7
DRF2PB05AA00EB	5	A	E	13
DRF2PB07AA00WB	7	A	W	2
DRF2PB07AA00EB	7	A	E	14
DRF2PB09AA00WB	9	A	W	3
DRF2PB09AA00EB	9	A	E	1
DRF2PB11AA00WB	11	A	W	6
DRF2PB11AA00EB	11	A	E	5
DRF2PB13AA00WB	13	A	W	1
DRF2PB13AA00EB	13	A	E	3
DRF2PB15AA00WB	15	A	W	4
DRF2PB15AA00EB	15	A	E	15
DRF2PB15AA01WB	15	A	W	10
DRF2PB17AA00EB	17	A	E	5
DRF2PB17AA00WB	17	A	W	0
DRF2PB19AA00EB	19	A	E	15
DRF2PB19AA00WB	19	A	W	7
DRF2PB13AA01EB	13	A	E	6
DRF2PB13AA01WB	13	A	W	0
DRF2PB13AA02EB	13	A	E	3
DRF2PB13AA02WB	13	A	W	0
DRF2PB05AA00EN	5	A	E	3
N/A	5	A	W	20
DRF2PB05AA01EN	5	A	E	9
DRF2PB05AA01WN	5	A	W	0
DRF2PB07AA00EN	7	A	E	13
DRF2PB07AA00WN	7	A	W	3
DRF2PB05AA00ES	5	A	E	5